Novel Approach for Computational Modeling of a Non-Premixed Rotating Detonation Engine

Sathyanarayanan Subramanian

Thesis submitted to the faculty of the
Virginia Polytechnic Institute and State University
in partial fulfillment of the requirements for the degree of

Master of Science
in
Mechanical Engineering

Joseph W. Meadows - Chair
Diana N. Biaraktrova
Danesh K. Tafti
Luca Massa

28th of June - 2019
Blacksburg, Virginia

Keywords: Rotating Detonation Engine (RDE), Non-Premixed Combustion, Computational Fluid Dynamics (CFD)

Novel Approach for Computational Modeling of a Non-Premixed Rotating Detonation Engine

Sathyanarayanan Subramanian

ABSTRACT

Detonation cycles are identified as an efficient alternative to the Brayton cycles used in power and propulsion applications. Rotating Detonation Engine (RDE) operating on a detonation cycle works by compressing the working fluid across a detonation wave, thereby reducing the number of compressor stages required in the thermodynamic cycle. Numerical analyses of RDEs are flexible in understanding the flow field within the RDE, however, three-dimensional analyses are expensive due to the differences in time-scale required to resolve the combustion process and flow-field. The alternate two-dimensional analyses are generally modeled with perfectly premixed fuel injection and do not capture the effects of improper mixing arising due to discrete injection of fuel and oxidizer into the chamber. To model realistic injection in a 2-D analysis, the current work uses an approach in which, a Probability Density Function (PDF) of the fuel mass fraction at the chamber inlet is extracted from a 3-D, cold-flow simulation and is used as an inlet boundary condition for fuel mass fraction in the 2-D analysis. The 2-D simulation requires only 0.4% of the CPU hours for one revolution of the detonation compared to an equivalent 3-D simulation. Using this method, a perfectly premixed RDE is comparing with a non-premixed case. The performance is found to vary between the two cases. The mean detonation velocities, time-averaged static pressure profiles are found to be similar between the two cases, while the local detonation velocities and peak pressure values vary in the non-premixed case due to local pockets fuel rich/lean mixtures. The mean detonation cell

sizes are similar, but the distribution in the non-premixed case is closer due to stronger shock structures. An analytical method is used to check the effects of fuel-product stratification and heat loss from the RDE and these effects adversely affect the local detonation velocity. Overall, this method of modeling captures the complex physics in an RDE with the advantage of reduced computational cost and therefore can be used for design and diagnostic purposes.

Novel Approach for Computational Modeling of a Non-Premixed Rotating Detonation Engine

Sathyanarayanan Subramanian

GENERAL ABSTRACT

The conventional Brayton cycle used in power and propulsion applications is highly optimized, at cycle and component levels. In pursuit of higher thermodynamic efficiency, detonation cycles are identified as an efficient alternative and gained increased attention in the scientific community. In a Rotating Detonation Engine (RDE), which is based on the detonation cycle, the compression of gases occurs across a shock wave. This method of achieving high compression ratios reduces the number of compressor stages required for operation. In an RDE (where combustion occurs between two coaxial cylinders), the fuel and oxidizer are injected axially into the combustion chamber where the detonation is initiated. The resultant detonation wave spins continuously in the azimuthal direction, consuming fresh fuel mixture. The combustion products expand and exhaust axially providing thrust/mechanical energy when coupled with a turbine.

Numerical analyses of RDEs are flexible over experimental analysis, in terms of understanding the flow physics and the physical/chemical processes occurring within the engine. However, three-dimensional numerical analyses are computationally expansive, and therefore demanding an equivalent, efficient two-dimensional analysis. In most RDEs, fuel and oxidizer are injected from separate plenums into the chamber. This type of injection leads to inhomogeneity of the fuel-air mixture within the RDE which adversely affects the performance of the engine. The current study uses a novel method to effectively capture these physics in a 2-D numerical analysis. Furthermore, the performance of the combustor is compared between perfectly premixed injection and discrete, non-premixed injection. The method used in this work can be used for any injector design and is a powerful/efficient way to numerically analyze a Rotating Detonation Engine.

ACKNOWLEDGMENTS

I extend my gratitude to my research advisor, Dr. Joseph Meadows for his guidance and support through my research project. Dr. Meadows helped me improve my problem-solving skills and he is a source of inspiration in my professional life. I thank Dr. Danesh Tafti, and Dr. Luca Massa for serving in my committee.

I am highly grateful to Dr. Diana Biaraktrova for providing me an opportunity to work as a Graduate Research Assistant in her research group, ACE(D) and for serving in my committee. Completion of my Master's degree might not have been successful without the support of Dr. Biaraktrova. I would also like to thank Dr. Scott Huxtable for his support in the vObjects project. I am grateful to Dr. Srinath Ekkad who had given me the opportunity to pursue my Master's degree at Virginia Tech.

I thank the Advanced Research Computing (ARC) department of Virginia Tech for providing computational resources in their cluster to run the CFD simulations. I am grateful to Dr. Brent Rankin of the Air Force Research Laboratory (AFRL), for providing the geometric model (CAD) used in their experiments for the current research. Special thanks to Piyush Raj for his inputs in post-processing and to Yamini Gaur for helping me troubleshoot my Java codes. I want to thank my lab colleagues Cody Dowd, Steven Wong, Ashwin Kumar, and Joseph Giroux for providing me technical suggestions, and for making our lab a conducive place to learn and fun to work.

My Master's program wouldn't have been a smooth sail without my friends here at VT, Shri Hari (primarily), Sachin, RK, and Chidambaram; and friends back home: Ganesh, Abhishek, Namitha, Pranav, Joby, Vigney, Aravind, VK, Yaseen, Ebin, Ravi, and the entire group. I am grateful to Mr. Mahil Yadin, Mr. De' Silva, Mr. Christopher, Dr. Chandramouli, Dr. Pugazenthi, Dr. Rafael Ruiz, Dr. Ricard Consel, Dr. Jordi Cadafalch, Dr. Prasad, Ms. Devi Kompella, and Mr. Les Baert for providing guidance/inspiration through my academic and professional career, helping me to be where I am now.

I wouldn't have come this far in my life without the love and support of my family. Thank you, Appa, Amma, Shuba, Pranesh, and Samara. *Ultimately, I bow to the creator*.

Table of Contents

Chapter 1: Novel Approach for Computational Modeling of a Non-Premixed Rotating Detonation Engine

LIST OF FIGURES

LIST OF TABLES

CHAPTER 1

Novel Approach for Computational Modeling of a Non-Premixed Rotating Detonation Engine

Sathyanarayanan Subramanian,[1] and Joseph Meadows.[2]
Department of Mechanical Engineering, Virginia Tech, Blacksburg, Virginia, 24060, USA

Submitted to the Journal of Propulsion and Power

Abstract

Pressure Gain Combustion (PGC) has gained significant attention in air-breathing gas turbine applications due to its increased thermodynamic efficiency over a constant-pressure Brayton cycle. Rotating Detonation Engine (RDE) is a form of PGC, which has advantages over Pulsed Detonation Engines (PDE) in terms of continuous, rapid energy release. In most RDEs, fuel and oxidizer are injected into the combustion chamber from separate plenums leading to an inhomogeneous mixture in the reaction zone. In this paper, a novel approach is developed to model inhomogeneous injection of the fuel-oxidizer mixture in a 2-D CFD analysis, that replicates the actual injection in a 3-D geometry. A Probability Density Function (PDF) of the fuel mass fraction from a converged 3-D, non-reacting simulation is extracted and is used as a spatially and temporally varying inlet boundary condition in the 2-D simulation. Using this method, a numerical analysis is carried out to predict the flow characteristics, flow structures, and detonation cell size of a non-premixed

---

RDE, using H_2-air as the fuel-oxidizer mixture. The simulation results are validated against experimental results in the literature, and these results from the non-premixed RDE simulations are compared against a perfectly premixed RDE, under same operating conditions.

Nomenclature

A = Area of nozzle throat (m^2)

c_1 = Constant 1 for numerical schlieren calculations = 0.8

c_2 = Constant 2 for numerical schlieren calculations = 1000

e = Specific internal energy of the gas (J/kg)

L = RDE channel length (0.4596 m)

$\dot{m}$ = Mass flow rate of the mixture (kg/s)

M(P) = Mach number as a function of static pressure

MW = Molecular weight (g/mol)

NS = Numerical Schlieren

P = Static pressure (Pa)

P_{cr} = Critical pressure (Pa)

P_o = Total pressure at the inlet (Pa)

R = Mixture gas constant (J/kg-K)

S_{mass} = Mass flux source term (kg/m^2-s)

T = Gas temperature (K)

T_o = Total temperature (K)

u = Gas velocity (m/s)

w = RDE channel width (0.0076 m)

X = Mole fraction of the species

β = Angle of the oblique shock wave

∇ = Gradient of a scalar

γ = Ratio of specific heats

λ = Detonation cell size (mm)

ν = Specific volume (m^3/kg)

φ = Local equivalence ratio

ρ = Gas density (kg/m^3)

Subscripts

1 = Properties measured upstream of the detonation wave

2 = Properties measured downstream of the detonation wave

i = i^{th} species

max = Maximum field variable value in the domain

min = Minimum field variable value in the domain

Introduction

The constant-pressure Brayton cycle has long been the thermodynamic cycle used in power generation and propulsion applications. The technological advancement in this domain has predominantly been at the component level than at the cycle level to an extent that the Brayton cycle and its associated components have been highly optimized. In pursuit of higher thermodynamic efficiency, the use of detonation cycles has been studied as an alternative to the Brayton cycle. In a detonation cycle (which is close to a constant volume cycle), the compression of gases occurs across a shock wave, which reduces the number of compressor stages required to generate high pressure in the cycle, as required in Brayton cycles. The additional work obtained with smaller pressure ratios (Fig. 1) makes the detonation cycle an attractive field of research. The improvement in the thermal efficiency using Pressure Gain Combustion (PCG) employing the detonation cycle, is found to be about 20% higher than a Brayton cycle operating with the same pressure ratio [1].

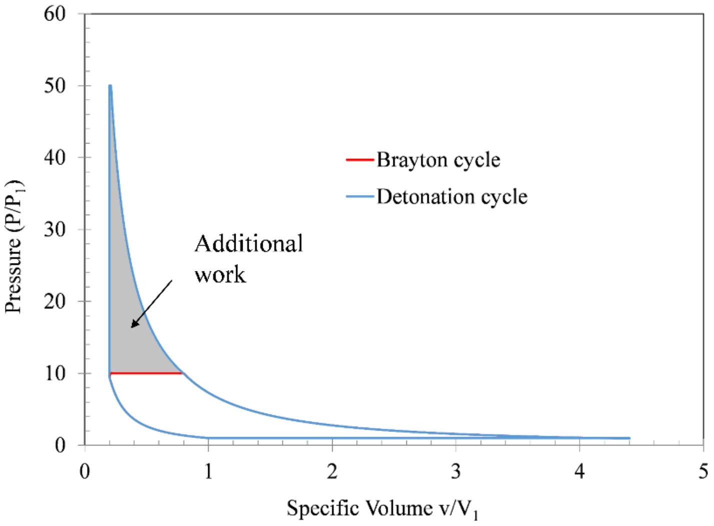

Fig. 1 Comparison of work done in a Brayton cycle with a Detonation cycle

Research on detonation engines started as early as 1940 when Zeldovich [2] proposed the use of detonation based combustion over deflagration due to the reduced entropy of the combustion products. It is reported [3] that Hoffman performed initial experiments, in the same year to check the feasibility of using detonation cycles for propulsion applications.

The experiments resulted in intermittent detonations and resulted in the birth of Pulsed Detonation Engines (PDEs). Rotating Detonation Engines (RDEs) gained more popularity as it provides continuous, quasi-steady output; requiring only one initiation of the detonation. In an RDE, the fuel-oxidizer mixture is axially injected (continuously) into an annular chamber where a detonation wave propagates continuously in the azimuthal direction, consuming the fresh reactant mixture. The combustion products then expand and exhausts, providing thrust or mechanical energy when coupled to a turbine.

A. Background and Objective

Detailed experimental investigation on RDE was conducted initially by Voitsekhovskii [4], starting from the 1960s. From then, multiple research groups have worked on the Research and Development of RDEs to understand various aspects of the RDE such as flow structures, propulsive performance, the effect of geometry, fuel, and injection methods on performance parameters, all of which are summarized in papers: [5-7]. Among the various parameters studied, the effect of fuel-oxidizer mixing on the performance of the engine is of high interest due to its adverse effects on the performance of the engine. Although injection of a perfectly premixed fuel-oxidizer mixture to the chamber provides advantages in terms of complete uniform combustion with higher combustion efficiency [8], it comes with certain drawbacks. High-pressure regions proceeding the detonation wave in the chamber may result in product backflow into the fuel and oxidizer plenums [9], which can damage the upstream injection components [10]. One approach to prevent product backflow is to design the fuel/oxidizer delivery system with chocked orifices. This approach limits the operability range and negates the benefit of pressure gain since it is suggested that the manifold pressure be a minimum of 2-3 times higher than the chamber pressure [11] to prevent flashback phenomenon. To overcome this issue, most RDEs are designed to have separate plenums for fuel and oxidizer injection, and these components are allowed to mix within the chamber (or slightly upstream) resulting in inhomogeneous mixture immediately downstream of the injector plane.

The fuel-oxidizer mixing process is identified to be crucial in sustaining continuous detonations [9] and poorly mixed fuel-oxidizers have shown effects similar to inert diluents [12]. Presence of inhomogeneous mixtures resulted in irregular detonation cell structures [13], skewed wavefront and reduced wave speeds [14] up to 6% [15]. Schwer and Kailasanath [16] investigated the effects of mixing due to different injector configurations and the results suggested that although the overall thrust did not vary significantly compared to an ideal case, the flow field was found to be complex. Imperfect mixing of fuel-oxidizer is found to drop instantaneous peak static pressures [17] and lead to instability of detonation wave [18]. Experimental analysis on the performance of an RDE for different fuel injection conditions also showed variation in wave speeds and detonation wave structures for different injection conditions [15, 19]. The peak detonation pressure and detonability of the mixture are also affected by the inhomogeneity of the reactant mixture [13]. Furthermore, numerical analysis of non-premixed RDE has revealed a reduced wave speed [20] and therefore a slight decrease in pressure gain. Recent high-fidelity simulations (both in 2-D and 3-D domains) indicate distortion of the wavefronts and its strength as a result of variation of local equivalence ratio (termed fuel-oxidizer stratification) [21].

Based on these analyses, it is evident that fuel-oxidizer mixing affects the detonation wave structure, detonation velocity, and pressure profiles (performance) of the RDE.

Numerical simulations of RDE provide additional flexibility over experiments in understanding the flow field, analyzing physical/chemical processes, and detonation wave structures which propagate at or near sonic speeds. Prior research that utilized numerical analyses to study the performance [22, 23], and understands the flow field [8, 24] of RDE, including the physics of inhomogeneous mixing effects, used expensive full-scale 3-D simulations. The challenge in using CFD to model RDE is primarily due to the large differences in time-scale between resolving the flow field and chemical reactions involved in the combustion process. Additionally, fine grid cells of the order of 10 to 100 microns may be required to accurately capture the features of the detonation wave, which make 3-D numerical simulations computationally expensive. Although advanced methods such as Adaptive Mesh Refinement (AMR) have been employed [22, 25] to overcome these challenges, the number of computational core hours required to resolve the flow field is still high. An alternate, inexpensive approach is to use an equivalent 2-D domain to model the RDE physics. In most cases, the 3-D domain is unrolled into an equivalent 2-D domain under the assumption that the radial gap between the coaxial cylinders is small compared to the diameter, and this diameter is large enough to not have any significant centrifugal forces affecting the flow [26]. Furthermore, the gradients of flow parameters along the radial direction are negligible compared to those in the axial and azimuthal directions in the domain. It was shown that both the three-dimensional and two-dimensional simulations provide similar results [27]. Initial numerical analysis in a 2-D domain was performed to understand the wave dynamics in an RDE [28] using a premixed H_2-O_2 mixture. Later, 2-D high-resolution Euler codes were used to predict wave speeds in a premixed RDE for different injection parameters (pressure and inlet area) [29] and for predicting the performance of the premixed RDE for various design parameters such as chamber length, and inlet pressures and temperatures [30]. Hishida [26] used a premixed 2-D model to understand the gas dynamics involved in an RDE. The research group of Schwer and Kailasanath [24, 31] employed an in-house 2-D numerical model that successfully predicted the flow field of a PDE to understand the effects of inlet stagnation pressure and injection geometries on the detonation structures in a premixed RDE. Rankin et al [32] used a low-fidelity 2-D premixed model to validate their time-averaged pressure profiles against their experiments to understand the flow field. Paxson et al [33] utilized a method in which the first few grid cells of the computational domain were made non-reacting to account for the mixing length, although the inlet mixture was perfectly premixed. In all these work, the inexpensive 2-D numerical model used the premixed injection and therefore did not capture the effects due to inhomogeneous mixing. To include the effects of fuel-oxidizer stratification in 2-D simulations, Fujii et al [34] used numerical source terms at different geometric locations to inject fuel and oxidizer separately and used this model to predict detonation velocities. Recently, Prakash et al [21] used a method in which a 3-D scalar field is generated with pockets of varying mixture fraction (equivalence ratio) which was mapped to a 2-D domain to achieve fuel stratification. The study compared the effects of fuel inhomogeneity on the wave structures for various degrees of fuel-oxidizer stratification using a Direct Numerical Simulation (DNS) approach, and it was observed that the fuel stratification affects the wave dynamics.

The present study bridges the gap in using inexpensive 2-D numerical analysis with a realistic approach of accounting for inhomogeneous mixture entering the RDE. The objectives of the current work are:

1) Numerically model inhomogeneity arising from discrete fuel-oxidizer injection by extracting a Probability Density Function (PDF) of the fuel mass fraction from a converged, 3-D, non-reacting simulation and use it as a spatially and temporally varying inlet boundary condition to the 2-D simulation. This method is validated against available experimental data from the literature.
2) A comparison of performance parameters (wave speed, pressure profiles, detonation height) and detonation wave structure (detonation cell size) is made between perfectly premixed and non-premixed RDEs.
3) The 2-D numerical method used in the current study does not account for heat loss from the RDE and reactant-product stratification arising from combustion product backflow. To check the effects of these physics on the detonation wave speed, an analytical method is used.

Computational Method

1. Geometry and Computational Domain

The geometry of the RDE (Fig. 2) used in the present study is based on the experimental setup used by Shank et al [35], which has also been used by various research groups. In this design, air and fuel are injected from separate plenums. Among the multiple design variations available in the setup, the current study utilizes the geometry with the height of the air injection slot of 0.89 mm. Fuel injection is through 120 evenly spaced injectors of hole diameter 0.71 mm located along the circumference (134 mm) of the combustion chamber. The outer and inner diameters of the chamber are 153.9 mm and 138.7 mm respectively. The height of the detonation channel is 101.6 mm. This 3-D geometry is used to simulate the cold-flow analysis from which the PDF of the fuel mass fraction is extracted for the 2-D simulation.

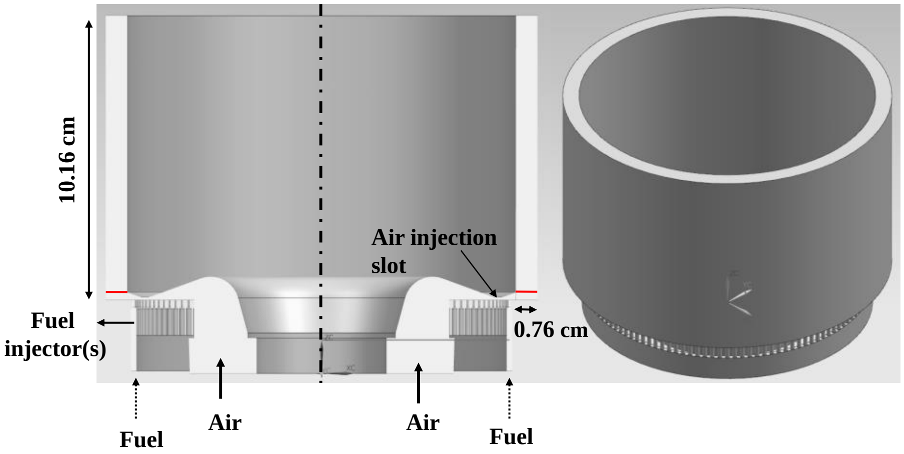

Fig. 2 Cross-sectional view (left) and isometric view (right) of the three-dimensional RDE geometry used for analysis

The PDF of the fuel mass fraction is extracted at the interface (marked in Fig. 2). Using this distribution as an inlet boundary condition, numerical analyses are carried out in the two-dimensional computational domain represented in Fig. 3. The 2-D domain is obtained by unrolling the toroidal section of the 3-D combustion chamber, such that the length of the domain is equal to the mean circumference of the 3-D geometry (45.96 cm), with the height retained at 10.16 cm. The air and fuel manifolds are omitted in the 2-D geometry. Therefore, to replicate the flow through the nozzle, numerical source terms are used at the inlet boundary, which is presented in the proceeding section.

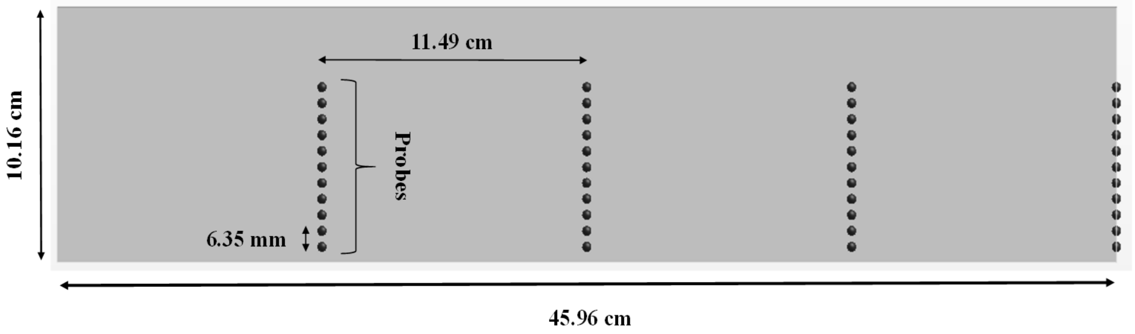

Fig. 3 Two-dimensional domain used for the numerical analysis

To measure the flow field parameters such as pressure, temperature, and wave speeds, multiple probes are placed at different axial locations similar to [19]. To measure the time-averaged static pressure at 11 axial locations from the inlet boundary, 4 sets (90^o apart in the azimuthal direction) of 11 probes each are placed along the axial direction (marked in Fig. 3). The probes are 6.35 mm apart axially, with the first probe located at 6.35 mm from the inlet boundary. Similarly, 4 additional probes (90^o apart in the azimuthal direction) are placed at an axial distance of 2.54 cm from the inlet boundary to measure instantaneous, peak pressures (these probes are not marked in the image).

2. Solver and Chemical Kinetics

To predict the flow field in the 3-D cold-flow simulations from which the Probability Density Function (PDF) is extracted, the steady state Reynolds-Averaged Navier Stokes (RANS) equations are solved. The governing equations of mass, momentum, energy and species conservation (Eq. (1) - (2)) are solved using the commercial solver, Star-CCM+, which uses the finite volume discretization method.

$$\frac{\partial}{\partial t}\int_V \boldsymbol{W}\,dV + \oint_A [\boldsymbol{F} - \boldsymbol{G}]\,.\,da = \int_V \boldsymbol{S}\,dV \tag{1}$$

$$where;\ \boldsymbol{W} = \begin{bmatrix}\rho \\ \rho v \\ \rho E\end{bmatrix},\ \boldsymbol{F} = \begin{bmatrix}\rho v \\ \rho vv + pI \\ \rho vH + pv\end{bmatrix},\ \boldsymbol{G} = \begin{bmatrix}0 \\ T + T_{RANS} \\ (T + T_{RANS}).\,v + \dot{q}''\end{bmatrix},\ \boldsymbol{S} = \begin{bmatrix}S_{mass} \\ S_{mom} \\ S_{ene}\end{bmatrix}$$

$$\frac{\partial}{\partial t}\int_V \rho Y_i\,dV + \oint_A \rho Y_i v\,.\,da = \oint_A \left[J_i + \frac{\mu_t}{\sigma_t}\,\nabla \mathrm{Y_i}\right].\,da \tag{2}$$

In the 3-D, steady-state, cold-flow simulation, Eq. (1) is solved with the transient and source terms (vector S) set to 0 in the cell control volume V which has a differential surface area da. ρ is the fluid density calculated using the ideal gas relation $\rho = p/RT$, v is the continuum velocity of the fluid, E is the specific total energy calculated as $E = H - p/\rho$ in which H = $C_pT + |v|^2/2$. The specific heat capacity C_p is calculated as a function of temperature given by the NASA polynomials of the *GRI-Mech 3.0* thermodynamic data file [36]. q'' is the heat flux term. The terms pI and T are the normal and shear stresses (viscous stress tensor). T_{RANS} is the shear stress due to the turbulent nature of the fluid flow. To resolve this turbulent flow, the SST k-ω (Menter) model [37] is used. In the species transport equation Eq (2), Y is the mass fraction of the species i, with only fuel H_2, and Air used at stoichiometric conditions in the cold-flow simulation. J_i is the laminar diffusive flux of the species calculated using the Fick's Law of diffusion, and μ_t and σ_t are the turbulent dynamic viscosity and turbulent Schmidt number respectively. A coupled flow, coupled energy solver with a third-order implicit, Monotonic Upstream-Centered Scheme for Conservation Laws (MUSCL) [38] is used for spatial discretization of the fluxes. The

3-D domain is discretized to ~7 million polyhedral cells with regions near the interface between the manifold and the channel further resolved to fine cells of the order of 100 microns. Using this setup, the 3-D case is simulated and the distribution of fuel mass fraction is extracted at a plane near the interface to be used as an input to the 2-D simulation.

To predict the reacting flow field in the 2-D domain, the unsteady Reynolds-Averaged Navier Stokes (uRANS) equations are solved (Eq (1) with the transient term). To include the creation and destruction of species in the species transport equation Eq. (2), the source term ω_i (species production rate) of each species is calculated as explained in [39]. Similarly, to model energy addition due to the reaction, chemical heat release rate is added as a source term to the energy equation (S_{ene} of Eq. (2)) which is calculated as the sum of the product of reaction rates [39] and the enthalpy of formation of all individual species. The detailed chemistry model with 9 species and 23 reactions based on a *reduced GRI-Mech 3.0* chemical mechanism [36] taken from CANTERA [40] is used to model these chemical kinetics involved in Hydrogen-air combustion. The transport properties and the specific heat capacities, which are a function of temperature, are also calculated using NASA polynomials provided by the *GRI-Mech 3.0* thermodynamic data file [36]. In addition to the SST k-ω (Menter) model [37] to predict turbulent flows, the laminar flame concept is used for turbulence-chemistry interaction. The 3rd order MUSCL scheme [38] is used for spatial discretization, primarily because, the MUSCL scheme (with a blending factor) in Star-CCM+ is a bounded scheme that switches between 3rd order upwind (during non-smooth flows/shock) and 3rd order central difference schemes (during smooth flow), which is suitable for flow with shocks in the domain. A 2nd order implicit backward differencing scheme is used for temporal discretization, which is neutrally stable at all courant (CFL) numbers and is less demanding computationally. The 2-D simulation is carried out in a structured grid of ~ 3.5 million cells, such that the grid cell size near the detonation region is 100 microns and gets coarser towards the exit plane up to a maximum size of 150 microns. A time step of 2.5×10^{-8} seconds is used. An MPI-based decomposition is used to parallel process the simulations and it takes about 1600 core-hours per revolution of the detonation wave. Data are post-processed and extracted after the detonation wave completes three revolutions and reaches a quasi-steady state.

3. Boundary Conditions

The 3-D and 2-D numerical analyses are carried out using specific operating conditions corresponding to the case 2.2.1.3 presented in [19], in which the global equivalence ratio is unity. In the 3-D cold flow simulation, mass flow boundary conditions are used to inject air and fuel from their respective plenums. Air is injected at 0.32 kg/s and fuel at 0.0093 kg/s with constant values of mass fractions to maintain a stoichiometric mixture inlet. The back pressure of the chamber is maintained at atmospheric conditions and the walls are treated adiabatic. The 3-D analysis is carried out using these boundary conditions and from the converged solutions of which the PDF of fuel mass fraction is extracted at the chamber-manifold interface and used in the 2-D simulation.

In the 2-D analysis, to replicate flow through the nozzle geometry in the experimental rig, the air-fuel mixture is injected into the combustion chamber using numerical source terms applied to the first row of grid cells. The H_2-air injection at the inlet boundary is governed by the downstream pressure in the RDE channel. In the absence of a detonation wave, the air-fuel mixture enters the domain at sonic conditions. At sonic conditions, the mass flux entering the RDE is based only on the critical pressure (P_{cr}) of the nozzle, calculated using Eq. (3)

$$\mathrm{P_{cr}} = \mathrm{P_o}\left(\frac{2}{\gamma + 1}\right)^{\frac{\gamma}{\gamma - 1}} \tag{3}$$

The total pressure (P_o) and total temperature at the inlet are set to 4.1 bar and 300 K respectively. Based on this critical pressure, the mass flux entering the chamber through the nozzle is calculated using the isentropic relation in Eq. (4).

$$\frac{\dot{m}}{A} = P_o \frac{\sqrt{\gamma}}{\sqrt{RT_o}}\, M(P)\left(\frac{1}{1 + \left(\frac{\gamma - 1}{2}\right) M(P)^2}\right)^{\frac{\gamma + 1}{2(\gamma - 1)}} \tag{4}$$

In Eq. (4), the area of the throat of the nozzle, *A* is measured to be 3.973 cm^2 from the experimental (3-D CAD) geometry. Using this area *A* in Eq. (4), gives a mass flow rate of 0.32 kg/s during choked conditions as in [19]. The local Mach number (M(P)) at the first row of cells, is governed by the cell static pressure (P) immediately downstream, which is calculated using Eq. (5)

$$M(P) = \sqrt{\left(\frac{2}{\gamma - 1}\right)\left(\left(\frac{P_o}{P}\right)^{\frac{\gamma - 1}{\gamma}} - 1\right)} \tag{5}$$

The value of downstream static pressure (P), which governs the flow of the mixture into the domain, is calculated based on one of the following conditions:

1) When $P > P_o$, the chamber is at a higher pressure compared to the manifold, and therefore the flow rate is set to zero. This is typically the case in the region (cells) of the domain where the high-pressure detonation wave is located.
2) When $P < P_o$ but $P > P_{cr}$, the flow at the throat is not chocked. The value of P in Eq. (5) takes the actual cell static pressure from the solver, from which the Mach number (M(P)) and the flow rate ($\dot{m}$) are calculated.
3) When $P \geq P_{cr}$, the flow is chocked, and P takes the value of P_{cr} in Eq. (5).

The mass flux source term for the 2-D domain (S_{mass}) at the inlet boundary is calculated using Eq. (6) that takes into account the RDE geometry. Eq. (6) is checked to ensure it accounts for the unit dimension in the 3rd coordinate (perpendicular to the paper) for the desired mass flow rate. Similarly, the momentum and energy source terms in the first row of cells with height Δy, are given by Eqs. (7-8)

$$S_{mass} = \frac{\dot{m}}{L.\mathrm{w}} \tag{6}$$

$$S_{mom} = \frac{\dot{m}u}{L.\mathrm{w}.\Delta\mathrm{y}} \tag{7}$$

$$S_{ene} = \frac{\dot{m}q}{L.\mathrm{w}.\Delta\mathrm{y}} \tag{8}$$

Where, u is the fluids velocity in the cell, and q is the total energy given by Eq. (9-10)

$$u = \sqrt{2C_pT_o[1 - \left(\frac{P}{P_o}\right)^{\frac{\gamma-1}{\gamma}}]} \tag{9}$$

$$q = C_p(T - T_{cell}) \tag{10}$$

The values of P in Eq. (9), follows the three conditions with respect to the critical pressure stated above. T_{cell} is the cell static temperature at the first row of cells, and Temperature, T in Eq. (10) is a function of Mach number, given by Eq. (11)

$$T = \frac{T_o}{1 + \left(\left(\frac{\gamma - 1}{2}\right) M(P)^2\right)} \tag{11}$$

Eqs. (3) to (6) provide the overall flow rate of the mixture entering the domain, however, the mass fraction of the individual species (hydrogen and air) entering the domain are not constant values. When the fuel and oxidizer are injected from separate manifolds (as in Fig. 2), the mixture at the inlet of the chamber is not perfectly premixed. To model the inhomogeneity of the fuel/air mixture in the 2-D analysis, a PDF of the fuel mass fraction is extracted at the inlet of the chamber (marked in Fig. 2) along the circumference of a 3-D non-reacting simulation. The PDF extracted for the current operating conditions is shown on the left of Fig. 4

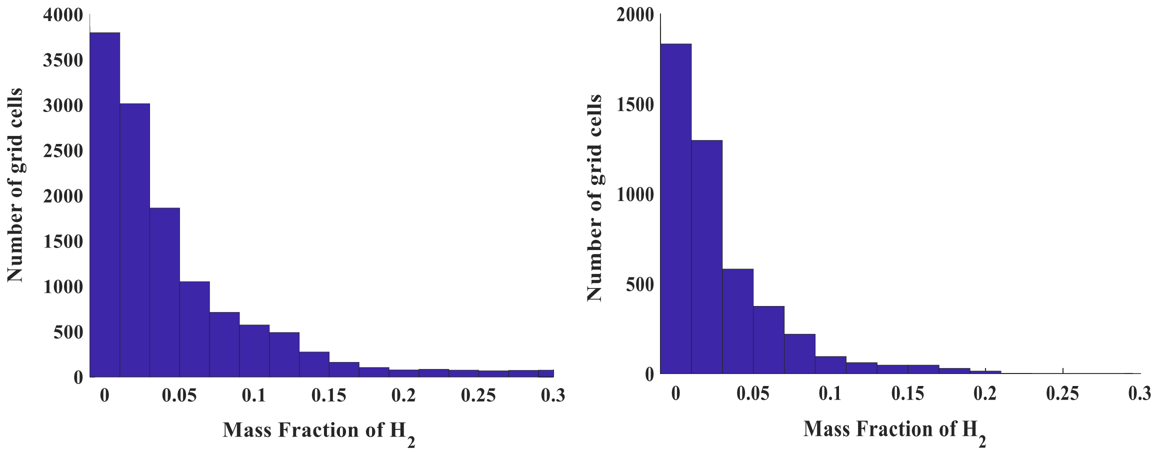

Fig. 4 Distribution of fuel mass fraction extracted from a non-reacting 3-D simulation (left) and the distribution reproduced that is provided as a boundary condition at the inlet of 2-D simulation (right)

To reproduce this PDF in the 2-D simulation, a Java code is developed to generate random numbers that are weighted to follow the distribution in the left of Fig. 4. These weighted random numbers are provided as H_2 mass fraction at the inlet boundary, and therefore replicating the inhomogeneity arising in the 3-D geometry. To generate weighted random numbers, the distribution from the 3-D simulation is divided into bins of suitable size and are stored as arrays along with their corresponding weights (whose sum is 1). The weight of each bin is multiplied by the number of grid cells in the first row of cells (4596 cells for a grid of 100 microns), to generate only the required number of random numbers. The equation Eq. (12), is looped based on the number of bins and the weight of each bin to replicate the distribution from the 3-D domain.

$$Random\ value = Bin_{left-edge} + \left(\left(Bin_{right-edge} - Bin_{left-edge}\right) * r.nextDouble\right) \quad (12)$$

Here, $Random\ value$ is the single random number generated whose value lies between the left and the right edge values of its corresponding bin. *r.nextDouble()* is a java built-in random number generator function, that generates uniformly distributed random numbers between 0 and 1. Therefore, with the number of random numbers generated equal to the number of cells in the first row cells, each cell is assigned a random number, which is the mass fraction of Hydrogen. Corresponding mass fraction values of oxygen and nitrogen are calculated to satisfy the total mass fraction value of unity. The assigned random numbers, and therefore the H_2 mass fractions at the inlet boundary are updated every three time-steps to model the spatial and temporal variation of the fuel mass fraction prevailing in the experiments. The global equivalence ratio is maintained at unity. The sample PDF obtained using the random number generator for a specific 2-D domain with a grid size of 100 microns is shown on the right of Fig. 4. The variation in local equivalence obtained using this method is highlighted in Fig. 5.

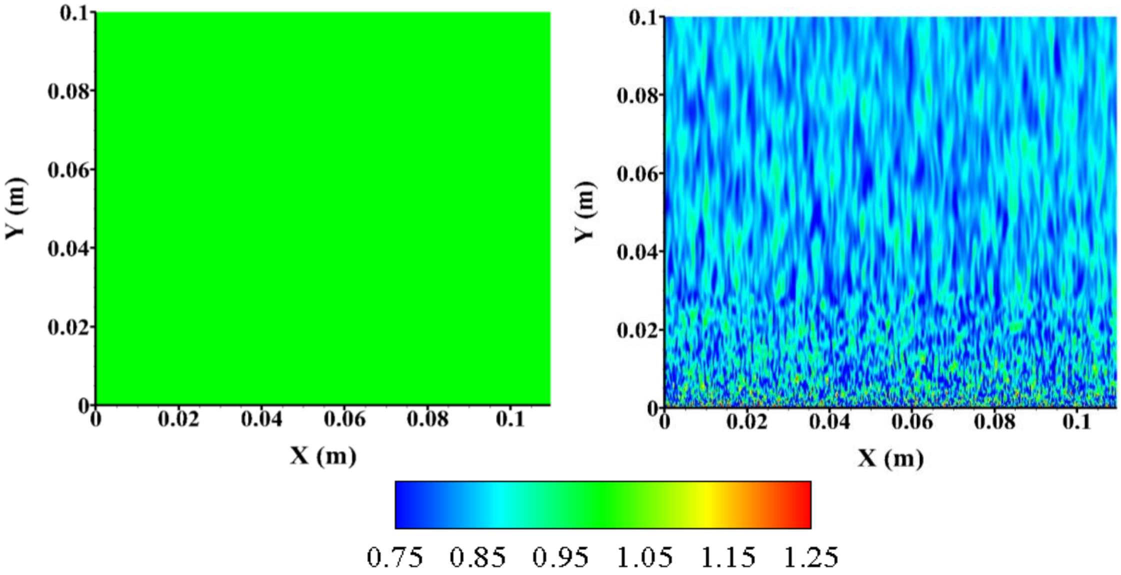

Fig. 5 Contours of equivalence ratio (before ignition) in a *section* of the 2-D domain obtained using the PDF method. *Left* – Premixed case; *Right* – Non-premixed case

With these conditions at the inlet, the outlet pressure boundary is set at atmospheric conditions. The left and the right boundaries are modeled as periodic interfaces to model wave propagation in the azimuthal direction.

4. Detonation Velocity Calculations

To compute the theoretical Chapman-Jouguet (CJ) velocity (u_1), the following system of non-linear equations Eqs. (14) - (16) are solved. These equations are conservation equations of mass, momentum, and energy with the condition that the products immediately upstream of the detonation wave is at sonic conditions [41]. These equations are solved for the Hydrogen-air chemical reaction given by Eq. (13). The system of non-linear equations is solved by employing an algorithm based on non-linear least-squares with large scale optimization [42]. The algorithm is based on interior Newton method [43] and is a subspace trust region method. CANTERA functions [40] are used to equilibrate the reactions and to determine the properties at each state, using the reduced GRI mechanism used in the CFD simulations.

$$H_2 + 0.5\ (O_2 + 3.76\ N_2) \rightarrow\ Equilibrium\ Products \tag{13}$$

$$u_1 = \frac{\rho_2}{\rho_1}\sqrt{\gamma_2 R_2 T_2} \tag{14}$$

$$e_2 - e_1 = 0.5\frac{(p_2^2 - p_1^2)}{\gamma_2 p_2 \rho_2} \tag{15}$$

$$p_2 = \left(\frac{\rho_2}{\rho_1}\right)\left(\frac{R_2 T_2}{R_1 T_1}\right) p_1 \quad (16)$$

The properties of the reactants (subscript 1) are measured at a temperature and pressure of 298 K and 1 atmosphere respectively, which are the values used in the CFD analysis. The mole fractions are taken as dictated by Eq. (13).

5. Grid Sensitivity Analysis and Validation with Experiments

To ensure spatial or grid independence of the flow field parameters, a grid convergence study is performed using meshes of 4 different sizes: 300 microns, 100 microns, 75 microns, and 50 microns. The Grid Convergence Index (GCI) (calculated for the first 3 sizes) gives a measure of the discretization error. To calculate the discretization error, mass fraction of H_2O (product) is chosen as the variable of interest, which is indicative of the species transport in the flow field after combustion, a method (parameter) similar to that used in [44] and [45]. The values of mass flow averaged H_2O mass fraction is taken along a plane at an axial location of 0.0508 m (mid-plane) for the analysis. The parameters and the calculation used for the GCI analysis is shown in Table 1, with equations explained in [46]. Here r is the refinement ratio, h is the inverse of cell size, p is the apparent order, e_a is the approximate relative error, and e_{ext} is the extrapolated relative error.

Table 1Parameters and calculations for grid independence analysis

Parameter / Equation	Value	Parameter / Equation	Value
Y_1	0.23777	$Y_{ext}^{21} = (r_{21}^{p} Y_1 - Y_2)/(r_{21}^{p} - 1)$	0.2376158
Y_2	0.23799	$Y_{ext}^{32} = (r_{32}^{p} Y_2 - Y_3)/(r_{32}^{p} - 1)$	0.2379757

Y_3	0.23854	$e_a^{21} = \lvert\frac{Y_1 - Y_2}{Y_1}\rvert$	0.000950090%
$r_{21} = h_2/h_1$	1.33333	$e_a^{32} = \lvert\frac{Y_2 - Y_3}{Y_2}\rvert$	0.002282842%
$r_{32} = h_3/h_2$	3.0000	$e_{ext}^{21} = \lvert\frac{Y_{ext}^{21} - Y_1}{Y_{ext}^{21}}\rvert$	0.000636021%
$\varepsilon_{21} = Y_2 - Y_1$	-0.0005433	$e_{ext}^{32} = \lvert\frac{Y_{ext}^{32} - Y_2}{Y_{ext}^{32}}\rvert$	0.000071739%
$\varepsilon_{32} = Y_3 - Y_2$	-0.0002259	$GCI_{fine}^{21} = \frac{1.25e_a^{21}}{r_{21}^p - 1}$	0.000794520%
$p = \frac{1}{\ln(r_{21})}\left\lvert\ln\left\lvert\frac{e_{32}}{e_{21}}\right\rvert + q(p)\right\rvert$	+3.1777797	$GCI_{fine}^{32} = \frac{1.25e_a^{32}}{r_{32}^p - 1}$	0.000089668%

The GCI index of 0.0008% and 0.00009% indicates the uncertainty of averaged H_2O mass fraction in terms of discretization error between the fine (75 microns) and medium (100 microns) grids. The discretization errors are sufficiently low in both the grid sizes of 75 microns and 100 microns. Additionally, the change in the mass fraction of H_2O (Fig. 6) is found to be less than 0.01% between the meshes of subsequent grid sizes.

In addition to the GCI index, the detonation velocities (Table 2), instantaneous (Fig. 7) and time-averaged pressure profiles (Fig. 8) are compared to ensure grid independence. The pressure gain (Fig. 7) and therefore the detonation velocities (Table 2) are found to be sensitive to the grid cell sizes, and are found to exceed the theoretical values of CJ velocity (column 3 of Table 2) and are closer to von-Neumann pressure, as the mesh cell sizes are reduced. Such sensitive behavior has been observed in prior research [47, 48] and conclusive reasoning for this phenomenon hasn’t been drawn yet. It has been observed that the reaction zone following the detonation wave exhibits significant spatial gradients on the order of 1-10 microns [49] and finer discretization is required to resolve detailed kinetics and viscous effects [50]. Powers et al [51] state that the finest length scale required to fully resolve the chemical kinetics and viscous effects is 0.1 microns. Resolving the kinetics and viscous effects at these length scales are computationally expensive and require high-fidelity simulation methods such as Direct Numerical Simulation with AMR, which are currently beyond the scope of this work; however, the method presented in the present study can be applied to various levels of modeling inhomogeneous fuel-oxidizer injection. As the simulation results obtained using a grid size of 100 microns reasonably predicts the physics such as wave structures, with values of peak pressures, and detonation wave speeds close to the theoretical conditions and satisfies the global mass balance in the domain, in addition to having a low discretization error value (Table 1), this mesh size (100 microns) is used for further analysis in this study. Several researchers [24, 30, 52] have used similar or larger grid cells to obtain insights on the flow physics. The time-averaged pressure and detonation velocity (experimental value is 84% of theoretical CJ velocity) are comparable with the experimental results.

Table 2 Detonation velocities at different grid size

Cell size (µm)	Detonation velocity (m/s)	% Theoretical CJ velocity
300	1915.12	97.234
100	1955.43	99.280
75	2034.45	103.293
50	2151.92	109.258

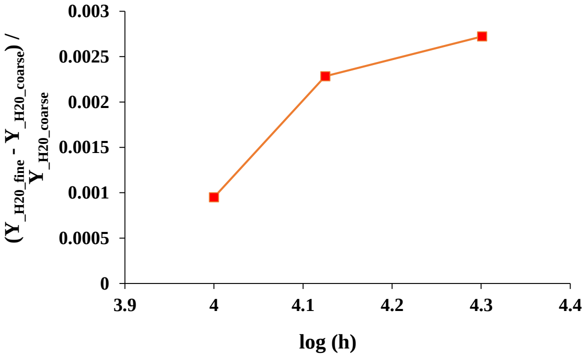

Fig. 6 Measure of detonation velocity as a function of h

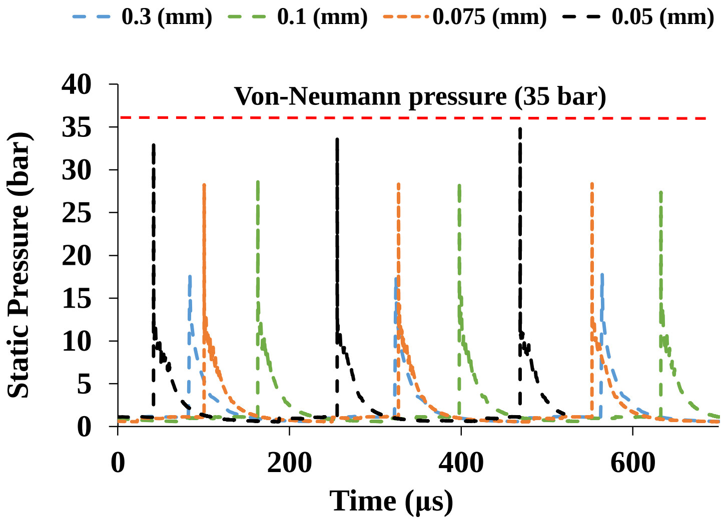

Fig. 7 Comparison of instantaneous pressure for different grid sizes

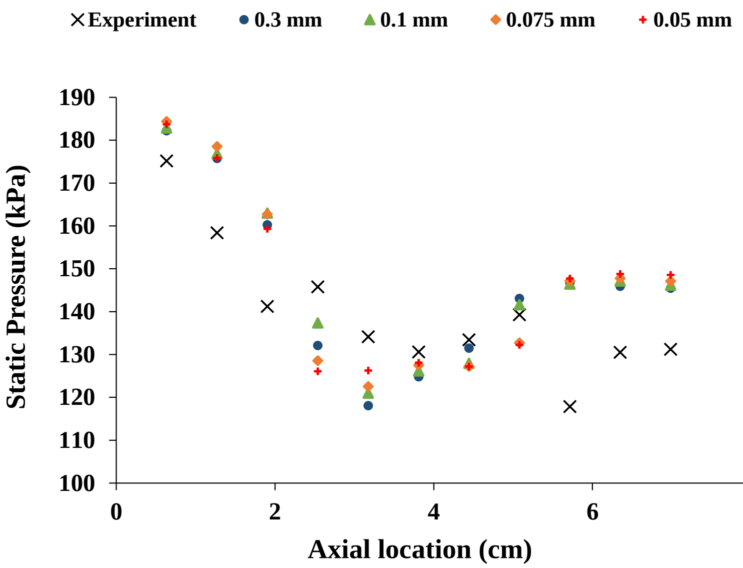

Fig. 8 **Comparison of time-averaged pressure for different grid sizes with experiment**

Results and Discussions

Utilizing this approach of using a PDF of fuel mass fraction at the inlet boundary to model inhomogeneity, the 2-D analysis of the RDE is carried out. Various parameters such as wave speeds, pressure profiles, work done, wave structure, and detonation cell sizes of the non-premixed RDE are studied and are compared with that of a perfectly premixed case in the section below.

1. Detonation Velocity, Pressure Profile, and Work Done

The detonation velocity in both the premixed and non-premixed (inhomogeneous) cases are measured at different time-steps using multiple probes marked in Fig. 3. Although the *mean* detonation velocity between the two cases does not change significantly (1957 m/s in premixed, and 1954 m/s in non-premixed), the instantaneous velocity measured at different time-steps changes drastically due to varying pockets of equivalence ratios in the non-premixed case (Fig. 9).

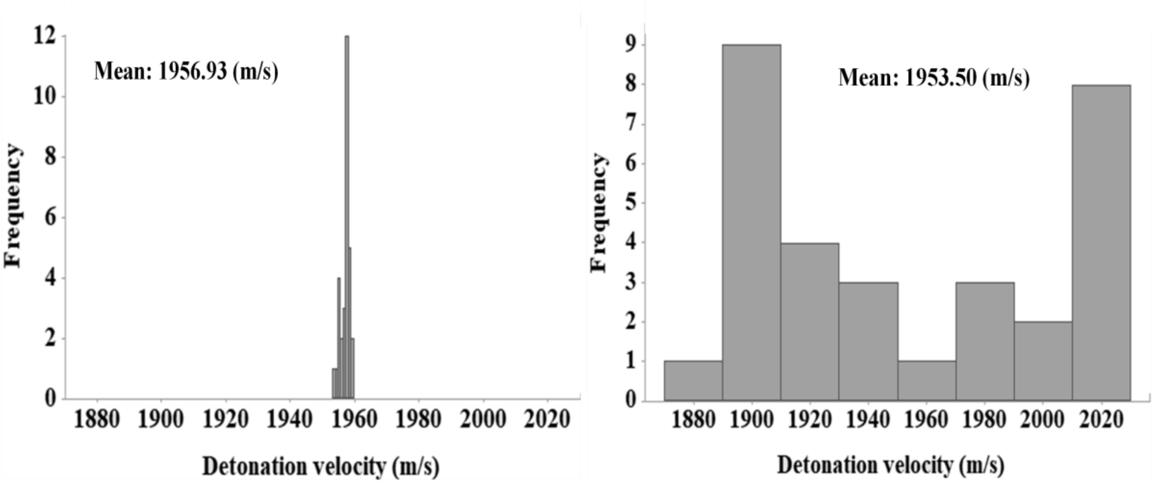

Fig. 9 Distribution of detonation velocities in premixed (left) and non-premixed (right) cases

In the non-premixed case, the extreme values of detonation velocities (in Fig. 9) of 1880 m/s and 2031 m/s correspond to a local equivalence ratio (φ) of ~0.85 and ~1.2 respectively, indicating the effect of inhomogeneity on the instantaneous wave speeds. The mean detonation velocity (listed in Table 3) obtained from the simulation is close to the theoretical value but is 20% higher than the experimental value [19]. Primary reasons for the higher velocity may arise by not considering the fuel-product stratification, due to product backflow mixing with the reactants, and heat loss from the RDE in the 2-D simulations. Their effects are analyzed in a later section.

Table 3 Comparison of detonation velocities

Case	Detonation velocity (m/s)	% CJ velocity	Frequency (kHz)
Theoretical CJ velocity	1976.7	-	4.272
Experiments [19]	1630	82.5	3.54
2-D premixed CFD	1957	99	4.230
2-D non-premixed CFD	1955	98.9	4.225

Comparing the time-averaged pressure profile (Fig. 10), the difference in the averaged pressure between the two cases is insignificant. Although Fig. 10 indicates that the average pressures are marginally higher in the premixed case up to an axial distance of 3 cm, (height of the detonation wave), the uncertainty indicated by the error bars (calculated using the standard error of the mean) clarifies that there is no significant difference between the two cases in terms of the time-averaged pressure profile.

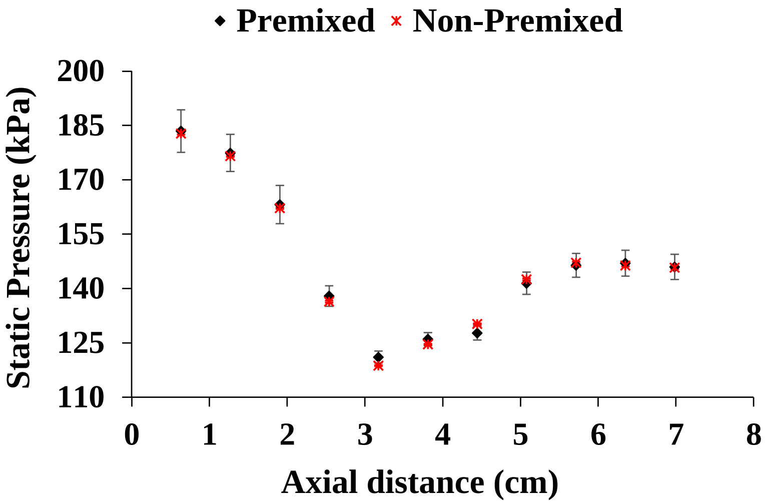

Fig. 10 Comparison of time-averaged pressure between premixed and non-premixed case

Similarly, comparing the instantaneous peak pressures (Fig. 11), the instantaneous values are mostly higher in the premixed case due to uniform mixing with an equivalence ratio of 1, however, at a few instances, similar to ~675 μs (circled and marked 3 in Fig. 11), the instantaneous pressure value becomes higher in the non-premixed case due to local pockets of fuel rich mixture (φ ~ 1.15) arising from the inhomogeneity, while the other peaks marked 1, 2, 4, and 5 are measured where the local fuel mixture is lean. In the non-premixed case, the local equivalence ratio is found to be lesser than unity at those times (~500 μs, ~625 μs, ~725 μs) leading to a relatively smaller pressure gain.

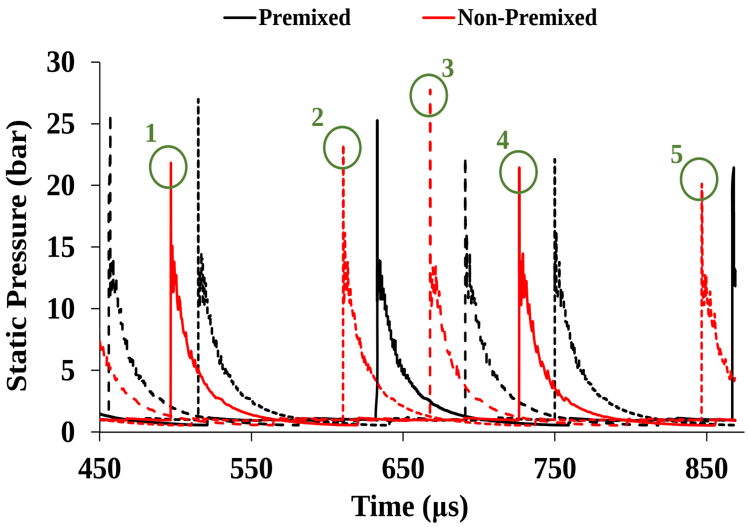

Fig. 11 Comparison of instantaneous pressure profiles between the premixed and non-premixed case

To compare the difference in the work done (therefore pressure gain) between the two cases, the area under the P-ν curve is calculated. To obtain the P-ν curve, the pressure (P) and specific volume (ν) are extracted along 5 streamlines (left of Fig. 12) which are drawn relative to a moving frame of reference traveling at the detonation velocity. Four of the five streamlines (marked 1 through 4 in Fig. 12) cross the detonation wavefront while the final streamline (marked 5) passes above the detonation wave which provides the work done due to the deflagration component of combustion.

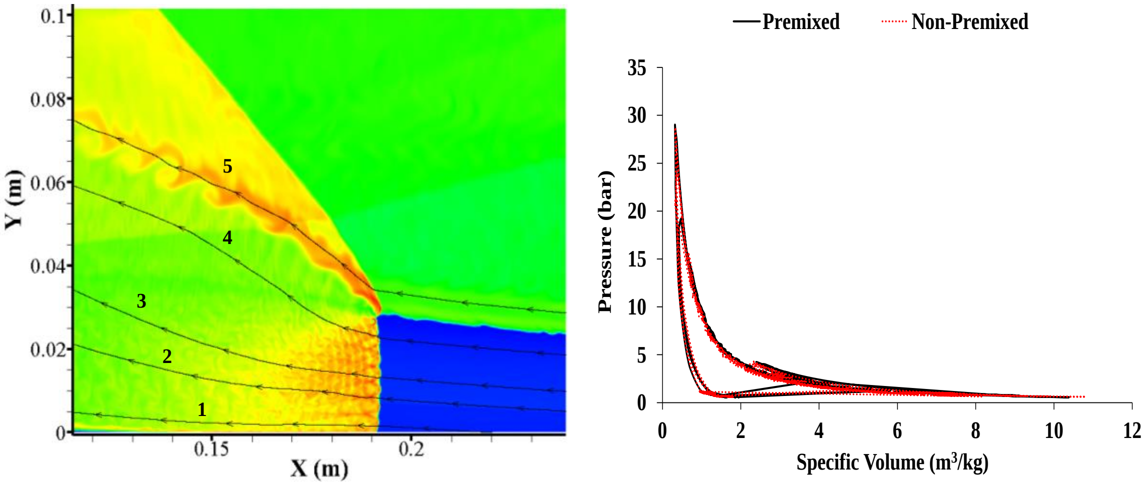

Fig. 12 ***Left*** **- Streamlines drawn to extract pressure and specific volume to calculate the work done.** ***Right*** **- Comparison of the work done between the premixed and non-premixed case**

Although the average work done (right of Fig. 12) is slightly higher in the premixed case (1880 kJ/kg) compared to the non-premixed case (1820 kJ/kg), the difference between the mean values are insignificant for the current operating conditions. This additional work is due to the higher pressure gain in the premixed case due to higher heat release from the uniform, stoichiometric mixture available for combustion, which will be discussed in the section on Variation of Performance Parameters with Local Equivalence Ratio.

2. Detonation Wave Structure

The detonation wave structure is studied by analyzing the numerical schlieren images from the simulations. To obtain instantaneous Numerical Schlieren (NS) plots, Eq. (17) below, taken from [53] is used during post-processing. In Eq. (17), ∇ρ is the gradient of gas density between the grid cells, c_1 and c_2 are constants that scales the density gradient to enhance flow field visualization. In the current analysis, values of c_1 and c_2 are 0.8 and 1000 respectively, which greatly enhances the small density gradients.

$$NS = c_1 \exp\left[\frac{-c_2(|\nabla\rho| - |\nabla\rho|_{min})}{(|\nabla\rho|_{max} - |\nabla\rho|_{min})}\right] \tag{17}$$

The height of the detonation wave is same across both the premixed and non-premixed cases (Fig. 13), justifying that the height is a function of stagnation pressure [31] and is unaffected by the inhomogeneity. The oblique shock is measured to be steeper in the premixed case with an angle (β in Fig. 13) of 51.64^o compared to 50^o in the non-premixed case, which results in higher expansion rates of products through the oblique shock region in the non-premixed case. Higher expansion through oblique shock results in increased entropy [54] and therefore higher thermodynamic loss [31] resulting in a loss in performance in the non-premixed case. Furthermore, the shear layer (marked *a* in Fig. 13), which is formed due to the interaction of combustion products of consecutive detonation waves, is dominant in the premixed case compared to an unstable slip line in the non-premixed one. The slip line governs the degree of expansion of the products, and a dominant slip region is found to reduce the thrust (performance) of the engine [55].

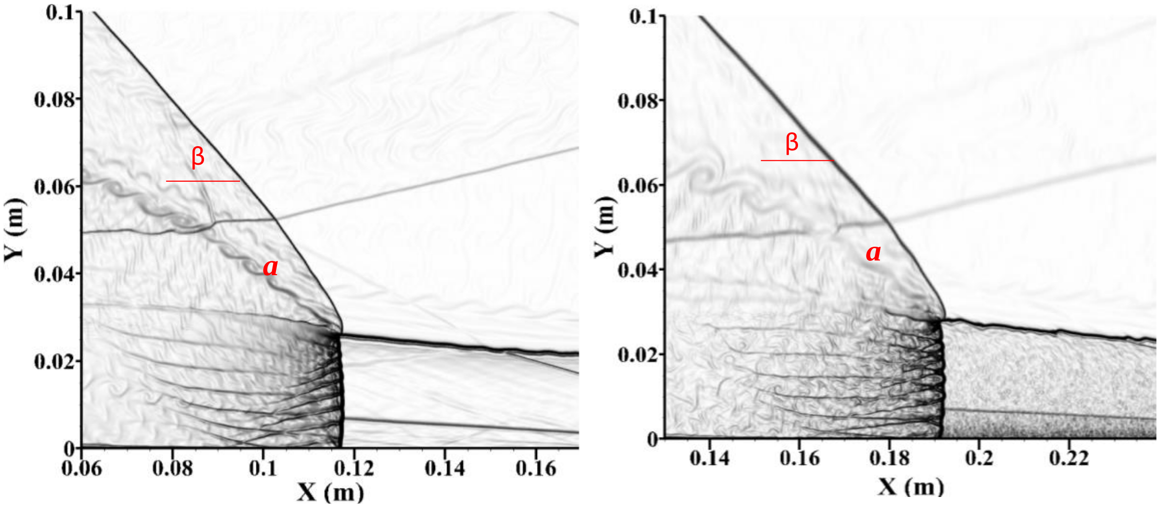

Fig. 13 Comparison of flow features between the premixed (left) and non-premixed (right) cases

The inhomogeneity of the mixture is also found to affect the local shape of the detonation wavefront. The fuel stratification has led to multiple, smaller *parabolic* detonation wavefronts as in the right of Fig. 14. The reaction front in the non-premixed case frequently detaches from the detonation shock structures due to pockets of rich and leaner mixtures, which leads to this type of *parabolic* wavefront. In the premixed case, the wavefront is smoother due to the homogeneous, stoichiometric mixture.

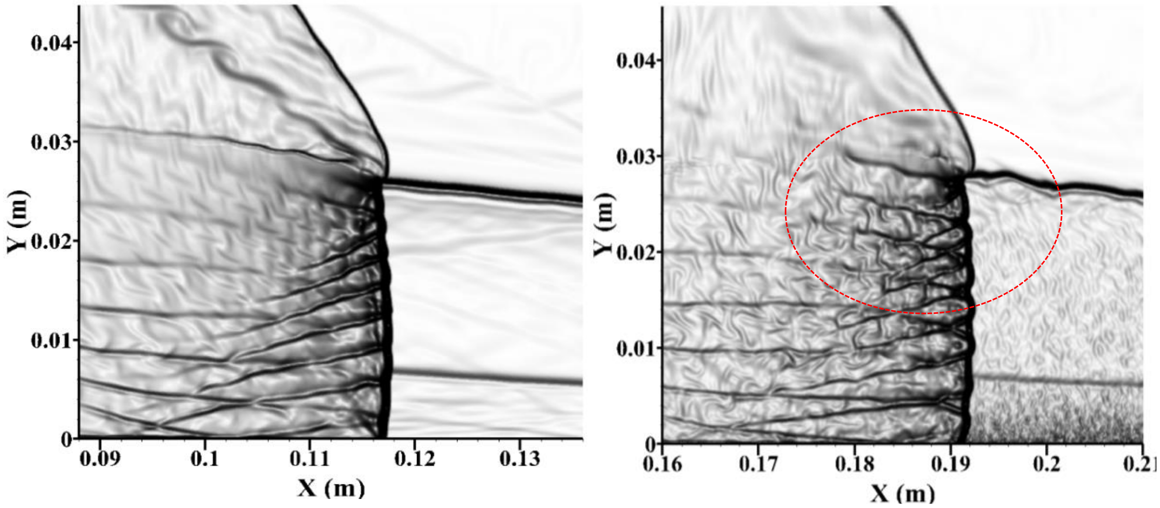

Fig. 14 Comparison of detonation wavefront between the premixed (left) and non-premixed (right) cases

3. Detonation Cell Sizes

An important parameter to determine the geometric dimension of an RDE is the detonation cell size, which is also affected by fuel stratification. Detonation cell size is the distance between two consecutive triple points stemming due to the interaction of the detonation wave, the oblique shock, and the reflected wave. Bykovskii [9] provides an important correlation between the detonation cell size (λ) and the minimum required dimensions of the RDE for the sustenance of the detonation wave as, minimum diameter $d = 30\lambda$, and width $= 2.5\lambda$. Furthermore, the minimum height of the fresh layer of reactant mixture required is also estimated using detonation cell size as $h \cong (12 \pm 5)\,\lambda$ by Bykovskii [9]. The detonation cell size of hydrogen is small compared to most hydrocarbon fuels [56], which is the primary reason for the interest in using H_2 as fuel in most RDEs [57]. In the current numerical analysis, the contours of detonation cell sizes are obtained by tracing the regions of maximum pressure downstream of the detonation wave. Using the measurement tool available in the commercial software, *ImageJ*, individual cell sizes are measured from these contours, and the mean value with corresponding distribution is calculated for the two cases. Furthermore, the mean detonation cell size value is validated using the code provided by Shepherd [58].

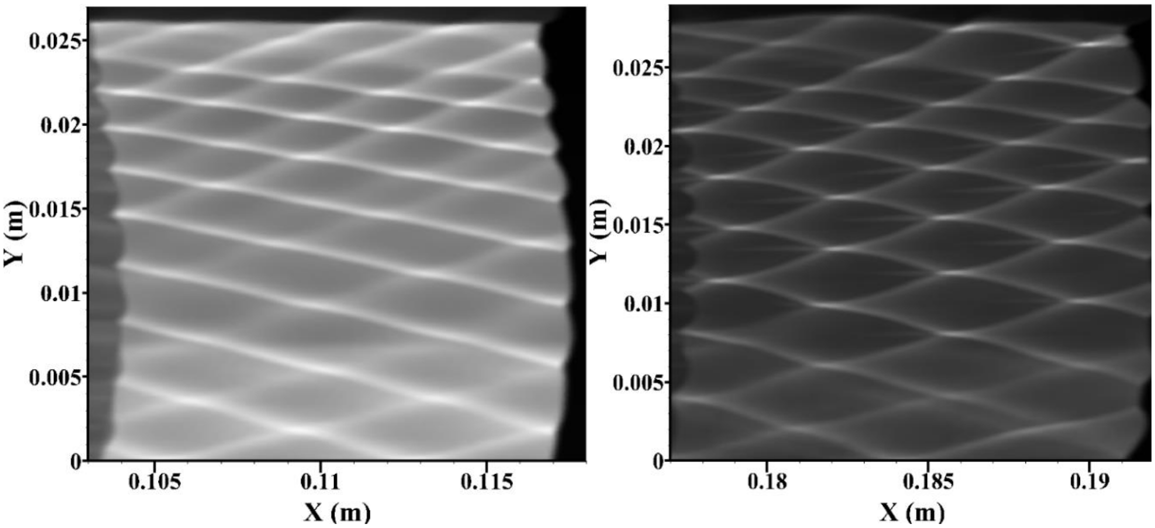

Fig. 15 Contours of detonation cell sizes in the premixed (left) and non-premixed (right) cases

The mean detonation cell size measured using the tool *ImageJ* gives values of 3.36 mm for the non-premixed case which is marginally higher compared to 3.30 mm in the premixed case. The mean values are close to the values provided in the literature [59] under current operating conditions. The mean values measured using Shepherd's code [58] are 3.895 mm and 3.825 mm respectively for the non-premixed and premixed cases. Shepherd's code is based on the idea that the detonation cells exhibit a periodicity (similar cell widths), and associates this periodicity with a relevant frequency and harmonics. These dominant frequencies are computed using Fourier Transform and the mean cell size is then calculated using only the relevant frequencies obtained using a power spectral density calculation, all of which are explained in [58]. However, in the current analysis, the cell sizes do not exhibit perfectly periodic behavior. In the non-premixed case, strong shock structures are observed farther from the inlet (circled in the right of Fig. 14), and therefore the cell size is large and uniform as we move away from the inlet towards the height of the detonation wave. Conversely, in the premixed case, the detonation cells farther away from the inlet boundary are smaller and less predominant (left of Fig. 15) due to weaker shock structures. This leads to a narrower distribution of the detonation cell size in the non-premixed case as in the right of Fig. 16.

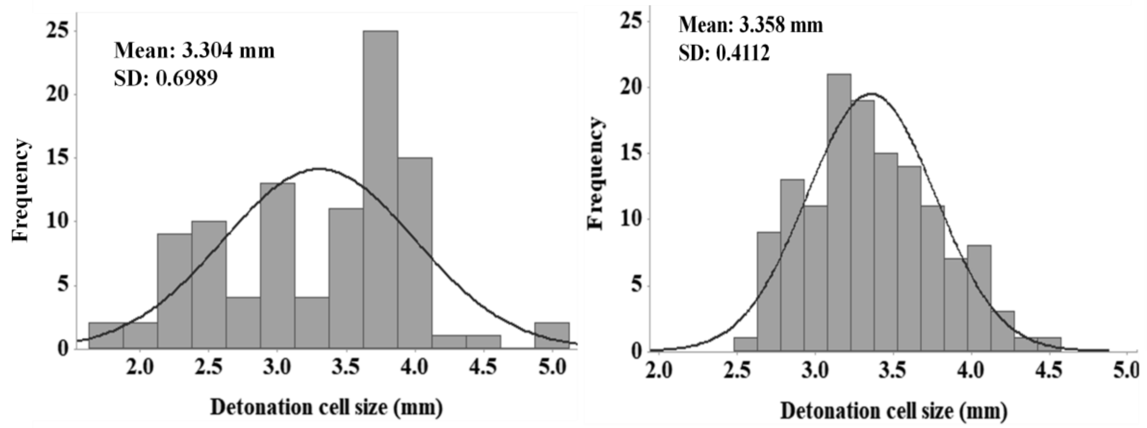

Fig. 16 Distribution of detonation cell sizes in premixed (left) and non-premixed (right) cases

4. Variation of Performance Parameters with Local Equivalence Ratio

To analyze the local variation of performance parameters as a function of local equivalence ratio (φ), metrics such as static pressure, heat release rate, temperature, and products mass fraction are extracted from a narrow region around the detonation wave, (marked in Fig. 17) at different time-steps and compared between the two cases.

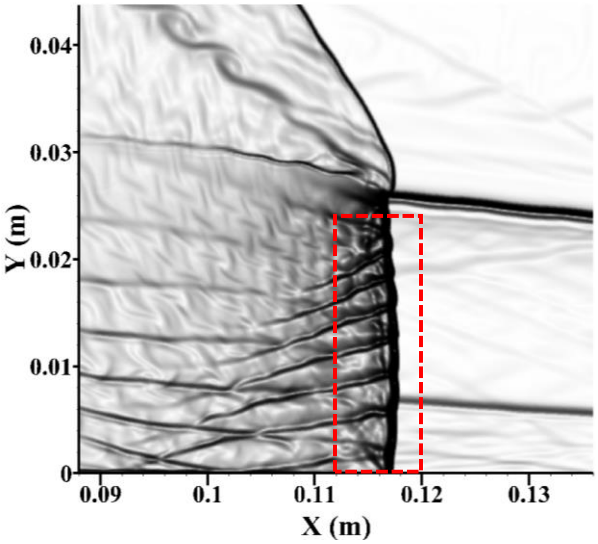

Fig. 17 Region of data extraction for comparison of performance parameters with equivalence ratio

The fraction of heat release is grouped under each bin of corresponding equivalence ratios (Fig. 18) to study the heat release occurring at rich and lean conditions. In the premixed case, the entire heat release occurs between an equivalence ratio range of 0.95 to 1.05, with ~48% of the heat release happening on the leaner side (0.95 to 1.00) with the remaining 52% of heat release is through a fuel rich mixture (1.00 to 1.05). In the non-premixed case, 87% of the heat release occurs at fuel lean conditions between equivalence ratios of 0.75 to 1.00 and the remaining 13% in the fuel rich regime between 1.0 and 1.2. This is the primary reason for the instantaneous peak pressures to be predominantly lower in the non-premixed case than the premixed in many instances (Fig. 11).

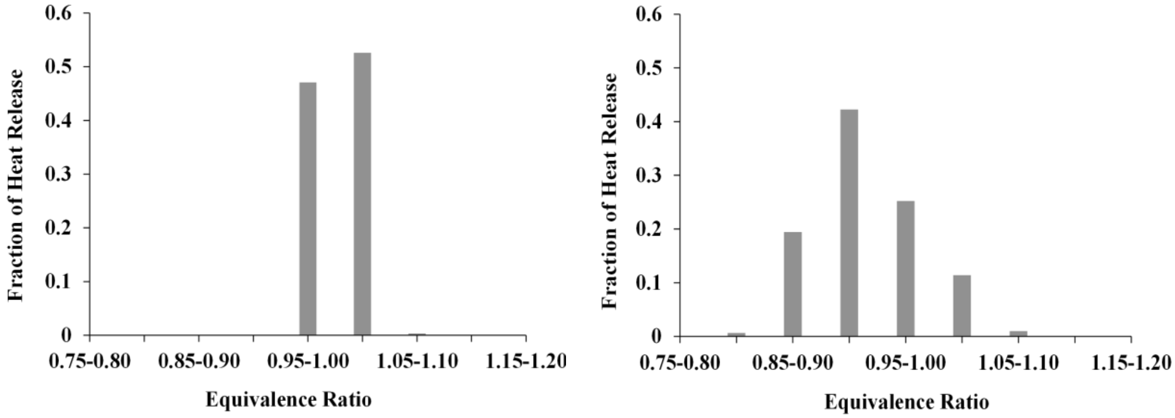

Fig. 18 **Comparison of heat release occurring at different equivalence ratios between the premixed (left) and non-premixed cases (right)**

Comparing heat release rates as a function of pressure (Fig. 19) gives the fraction of heat release that occurs as detonation (higher pressures). By considering a 5 bar pressure as a benchmark for high-pressure combustion [8], 0.2% of heat release occurs below this mark for the premixed case, compared to a highly negligible 0.07% in the non-premixed case. However, 37% of the heat release occurs at higher than 25 bar pressure in the premixed case compared to 32% in the non-premixed case, resulting in higher pressure gain in the premixed case.

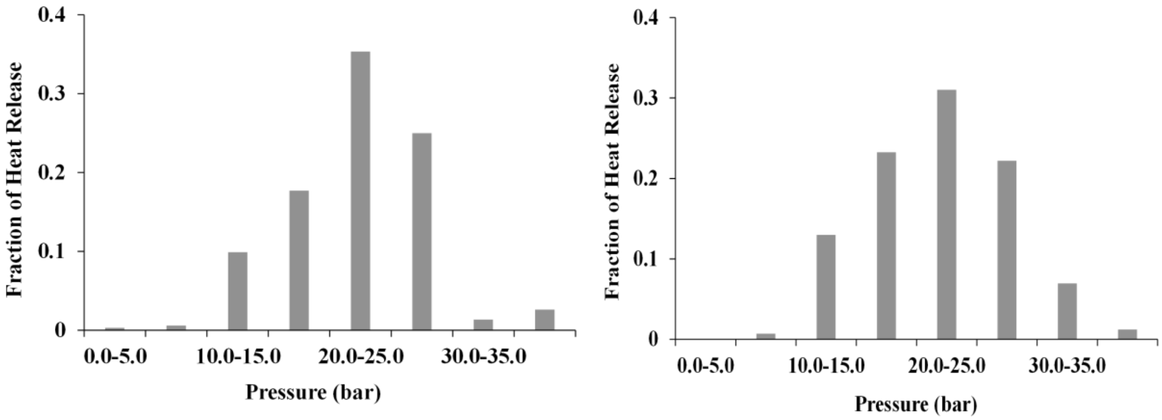

Fig. 19 **Comparison of heat release at different pressures between the premixed (left) and non-premixed (right) cases**

The variation of H_2O and OH mass fractions in the non-premixed case (b and d of Fig. 20) resembles the Zeldovich-von Neumann-Doring (ZND) profile, such that they vary linearly up to an equivalence ratio of 1.0 (marked with dotted lines in Fig. 20 b). Beyond this value, the mass fraction still increases but with a smaller gradient. In the premixed case (a and c of Fig. 20), although the data points are concentrated around an equivalence ratio of one, a similar relationship between the parameters can be drawn. Beyond an equivalence ratio of 1.0, although linear, the increase in the species mass fraction is more gradual compared to the range below the equivalence ratio of 1.0.

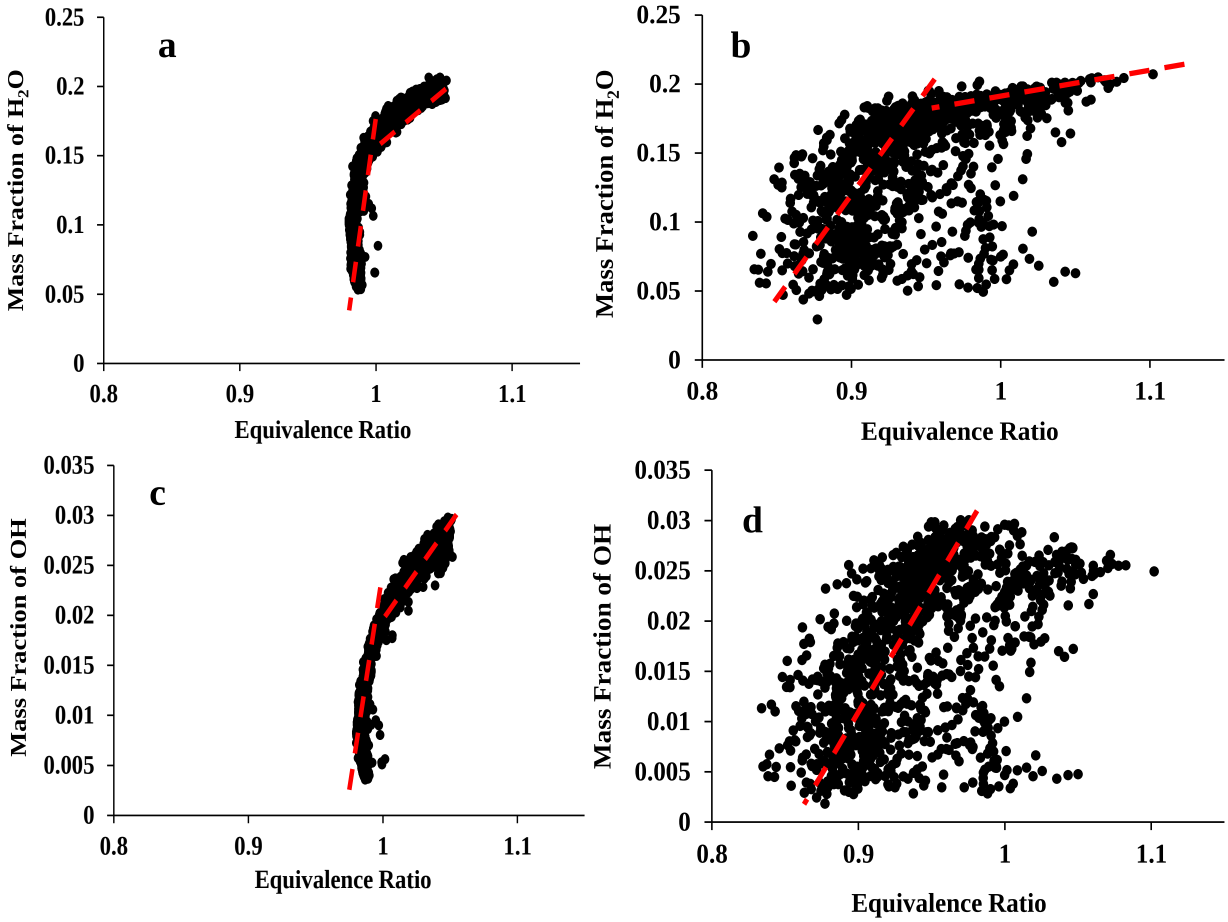

Fig. 20 Comparison of H_2O and OH mass fractions as a function of local equivalence ratio between premixed (left) and non-premixed (right) cases

In the non-premixed case, the variation of temperature is proportional to the equivalence ratio (Fig. 21 b) up to a value of 1.0, beyond which the temperature oscillates around this maximum value. Additional data points at higher equivalence ratios might be required to further investigate how the temperature varies at higher equivalence ratios, which are unavailable with the current simulation data. The heat release rates in the non-premixed case are spread for different equivalence ratios and no observable correlation exists. In the premixed case (Fig. 21 a), the temperature clearly is higher in regions of higher equivalence ratio, however, the range of equivalence ratio under analysis is too narrow (1.0 to ~1.05) to establish a concrete relationship between the two parameters.

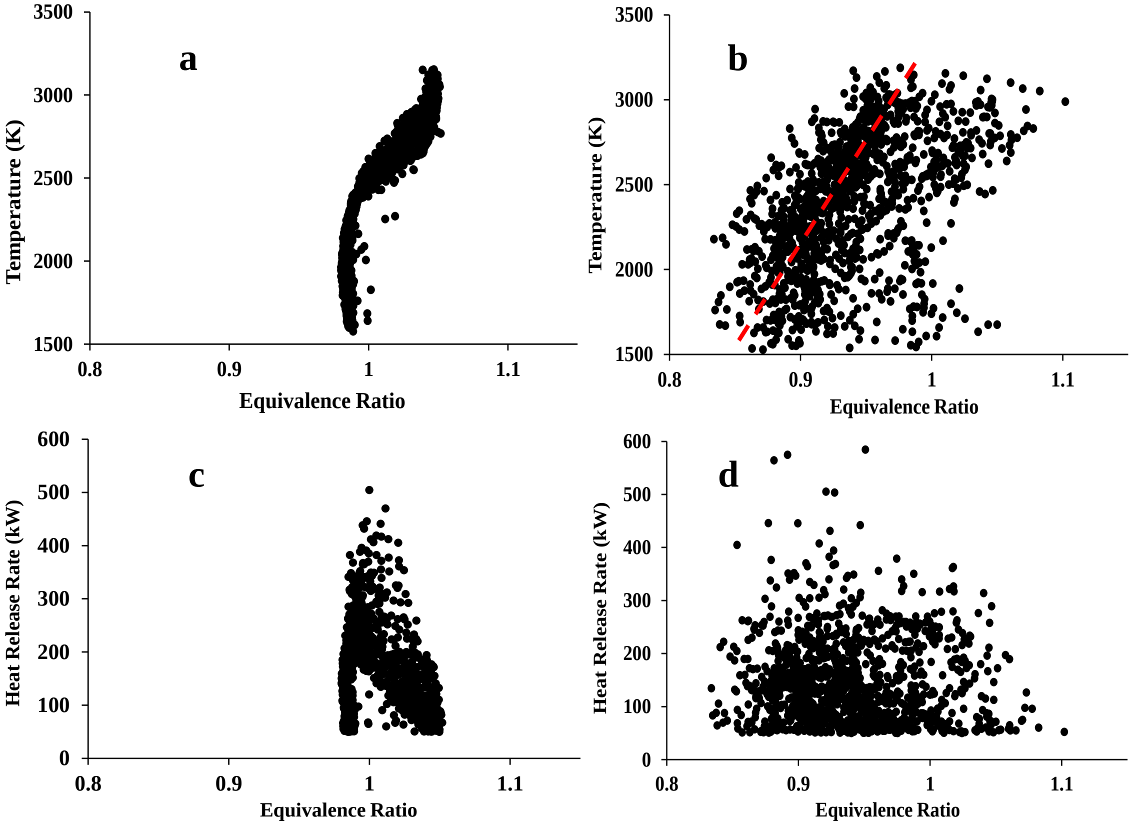

Fig. 21 Comparison of temperature and heat release rate as a function of local equivalence ratio between the premixed (left) and non-premixed (right) cases

5. Heat Loss and Fuel-Product Stratification

The detonation velocities in Table 3 highlights a gap between wave speeds obtained from the experiments [19] and the numerical analysis. The increased detonation velocities in the numerical analysis could arise from not considering the fuel-product stratification arising due to the backflow and re-entry of combustion products into the chamber, and the heat loss from the RDE. To check the impact of these two flow physics, a supplementary analytical method is used to predict their effects on the detonation wave speeds. To compute the modified detonation velocity (CJ_{strat}) due to fuel-product stratification, the chemical equilibrium equation Eq. (13) is modified to Eq. (18) to account for the combustion products mixed with the reactants at the inlet.

$$[H_2 + 0.5\ (O_2 + 3.76\ N_2)] + \ X[H_2O]\ \rightarrow Equilibrium\ Products \tag{18}$$

The theoretical detonation velocity is calculated by solving the system of equations Eqs. (14-16) for the equilibrium equation Eq. (18). To account for the heat addition due to backflow of products, the initial temperature used for the calculation is a mass-averaged value of the reactants and the products. The modified detonation velocity is calculated for different mass fractions of stratification (Y_{strat}) calculated as in Eq. (19)

$$Y_{strat} = \frac{X \cdot MW_{H_2o}}{\sum X_i \cdot MW_i} \tag{19}$$

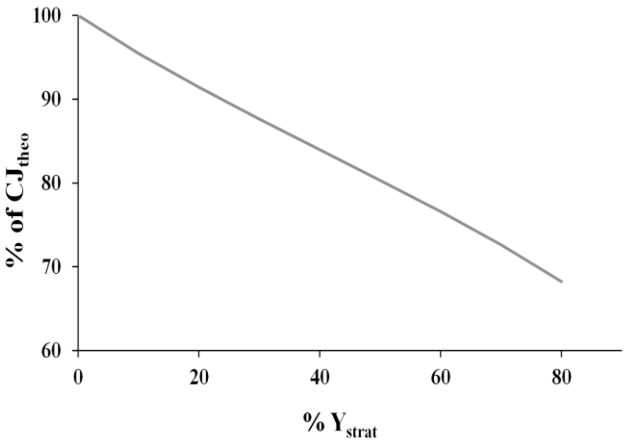

Fig. 22 Effect of fuel-product stratification on the detonation velocity

The detonation velocity is found to linearly decrease (Fig. 22) with the presence of combustion products diluting the fresh fuel mixture and drops up to approximately 70% of the theoretical velocity for 80% products in the reactant mixture.

Heat loss from the RDE is another deterrent to the performance of the engine. To measure the effect of heat loss on the detonation velocity, a modified version of the system of equations Eqs. (14-16) is solved in which a heat loss term (Q_{loss}) is added to Eq. (15) which then becomes Eq. (20)

$$e_2 - e_1 = 0.5\,\frac{(p_2^2 - p_1^2)}{\gamma_2 p_2 \rho_2} - Q_{loss} \tag{20}$$

Heat loss from the RDE also deters the detonation velocity (Fig. 23), although not as significant as fuel-product stratification. The detonation velocity is inversely proportional to the heat loss and it decreases to 90% of an adiabatic detonation wave for heat losses as high as 300 kW/kg of mixture.

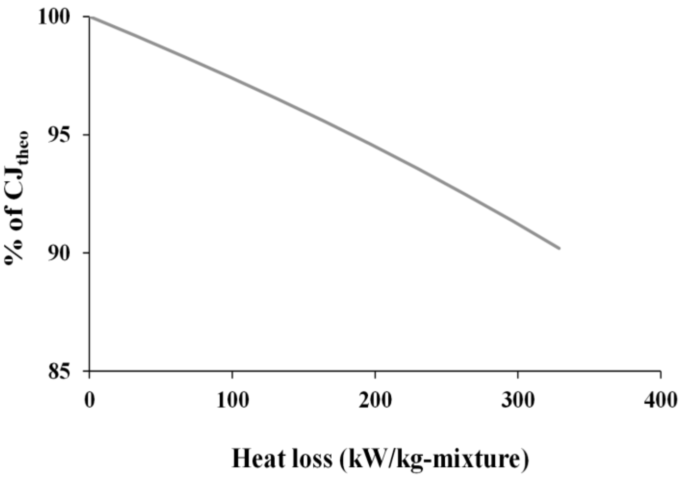

Fig. 23 **Effect of heat loss on the detonation velocity**

Conclusion

In the current work, a new technique is employed to model the inhomogeneity arising from discrete fuel-air injection in 3-D injection design into a 2-D numerical analysis. In this method, a Probability Density Function of the fuel mass fraction is extracted at the chamber inlet from a converged cold-flow 3-D simulation, and the extracted PDF is replicated by generating weighted random numbers and is provided as an inlet boundary for the 2-D simulation. Using this approach, a non-premixed RDE simulation is validated with experimental results available in the literature and is compared with that of an equivalent premixed case. Also, this approach reduces the computational time drastically compared to an equivalent 3-D simulation, such that it required only 0.3% of the resources. Based on the comparisons between the premixed and the non-premixed cases, it is found that the mean detonation velocity is very similar between the two cases, however, the local detonation velocity (and the distribution) varies significantly in the non-premixed case due to local pockets of rich/lean mixtures. Furthermore, the differences between time-averaged pressures in the premixed and non-premixed cases are negligible. On comparing the instantaneous peak pressures, the values in the non-premixed case are either higher/lower compared to the premixed case depending on the local equivalence ratio. On most occasions, the premixed case has a higher instantaneous peak pressure because 87% of the heat release is found to occur at fuel lean conditions in the non-premixed case. To compare the work done, five streamlines are drawn at various locations in the domain using a moving frame of reference along with the detonation wave, and values of Pressure and specific volume are extracted. On comparing the work done, only a slight decrease in work is observed in the non-premixed case. On analyzing the wave structures using numerical schlieren technique, the shock structures furthest away from the inlet and near the detonation wave are found to be stronger in the non-premixed case than in the premixed case, leading to a relatively even distribution of detonation cell sizes in the non-premixed case. Furthermore, the detonation wavefront in the non-premixed case is found to have local parabolic profiles due to the detachment of shock structures locally owing to pockets of rich/lean mixtures. In the premixed case, the wavefront is smoother. The shear layer in the non-premixed case is not as prominent as in the premixed case. Also, the angle of oblique shock is found to be steeper in the premixed case (51.64 degrees) compared to the non-premixed case (50 degrees). The detonation wave height is found to be equal in both the cases and reiterates that the detonation height is a function of inlet stagnation pressure only. The mean detonation cell size is slightly higher in the non-premixed case (3.36 mm), compared to the premixed case (3.304 mm). However, the detonation cell size farther away from the inlet boundary in the premixed case diminishes due to weaker shock structures. This leads to a wider spread in the distribution of the cell size. On comparing the effect of local equivalence ratio on the performance, the mean heat release in the premixed case occurs at an equivalence ratio of 1.02 compared to 0.96 in the non-premixed case, which is the primary reason for lower instantaneous peak pressures in the non-premixed case. Further, 87% of the heat release occurs in the fuel-lean side in the non-premixed case, compared to 48% in the premixed case. Also, in the premixed case, 37% of the heat release occurs at a pressure higher than 25 bar compared to 32% in the non-premixed case. The OH and H2O mass fractions resemble the ZND profile, such that they vary linearly with local equivalence ratio up to the value of 1, beyond which the variation is gradual. A similar trend is observed in both cases. The effects of fuel-product stratification and heat loss from the RDE are not included in the 2-D simulations and therefore their effects are checked using analytical methods. The fuel-product stratification has a significant impact on the detonation velocity compared to heat loss from the RDE, as the detonation velocity drops in both these cases. The effect of product diluents on the wave structure, detonation cell size, and heat release using high-fidelity simulations is a part of the future work of the research group.

References

1. Wintenberger, E., and Shepherd, J. "Thermodynamic Cycle Analysis for Propagating Detonations," *Journal of Propulsion and Power* Vol. 22, No. 3, 2006, pp. 694-698.
doi:10.2514/1.12775

2. Zeldovich, Y. B. "To the Question of Energy Use of Detonation Combustion," *Journal of Propulsion and Power* Vol. 22, No. 3, 2006, pp. 588-592.
doi:10.2514/1.22705

3. Nicholls, J., Wilkinson, H., and Morrison, R. "Intermittent Detonation as a Thrust-Producing Mechanism," *Journal of Jet Propulsion* Vol. 27, No. 5, 1957, pp. 534-541.
doi:10.2514/8.12851

4. Voitsekhovskii, B. "Stationary Spin Detonation," *Soviet Journal of Applied Mechanics and Technical Physics* Vol. 3, No. 6, 1960, pp. 157-164.

5. Kailasanath, K. "The Rotating Detonation-Wave Engine Concept: A Brief Status Report," *49th AIAA Aerospace Sciences Meeting including the New Horizons Forum and Aerospace Exposition*. 2011, AIAA 2011-580.
doi:10.2514/6.2011-580

6. Wolański, P. "Detonative Propulsion," *Proceedings of the Combustion Institute* Vol. 34, No. 1, 2013, pp. 125-158.
doi:10.1016/j.proci.2012.10.005

7. Lu, F. K., and Braun, E. M. "Rotating Detonation Wave Propulsion: Experimental Challenges, Modeling, and Engine Concepts," *Journal of Propulsion and Power* Vol. 30, No. 5, 2014, pp. 1125-1142.
doi:10.2514/1.B34802

8. Cocks, P. A., Holley, A. T., and Rankin, B. A. "High Fidelity Simulations of a Non-Premixed Rotating Detonation Engine," *54th AIAA Aerospace Sciences Meeting*. 2016, AIAA 2016-0125.
doi:10.2514/6.2016-0125

9. Bykovskii, F. A., Zhdan, S. A., and Vedernikov, E. F. "Continuous Spin Detonations," *Journal of Propulsion and Power* Vol. 22, No. 6, 2006, pp. 1204-1216.
doi:10.2514/1.17656

10. Thomas, L., Schauer, F., Hoke, J., and Naples, A. "Buildup and Operation of a Rotating Detonation Engine," *49th AIAA Aerospace Sciences Meeting including the New Horizons Forum and Aerospace Exposition*. 2011, AIAA 2011-602.
doi:10.2514/6.2011-602

11. Liu, S.-J., Lin, Z.-Y., Liu, W.-D., Lin, W., and Zhuang, F.-C. "Experimental Realization of H2/air Continuous Rotating Detonation in a Cylindrical Combustor," *Combustion Science and Technology* Vol. 184, No. 9, 2012, pp. 1302-1317.
doi:10.1080/00102202.2012.682669

12. Mikhalkin, V. "Thermodynamic Calculation of Detonation in Poorly Mixed Gas Mixtures," *Combustion, Explosion and Shock Waves* Vol. 32, No. 1, 1996, pp. 57-60.
doi:10.1007/BF01992192

13. Ettner, F., Vollmer, K., and Sattelmayer, T. "Mach Reflection in Detonations Propagating through a Gas with a Concentration Gradient," *Shock Waves* Vol. 23, No. 3, 2013, pp. 201-206.
doi:10.1007/s00193-012-0385-8

14. Ishii, K., and Kojima, M. "Behavior of Detonation Propagation in Mixtures with Concentration Gradients," *Shock Waves* Vol. 17, No. 1-2, 2007, pp. 95-102.
doi:10.1007/s00193-007-0093-y

15. Calhoon, W., and Sinha, N. "Detonation Wave Propagation in Concentration Gradients," *43rd AIAA Aerospace Sciences Meeting and Exhibit*. 2005, AIAA 2005-1167.
doi:10.2514/6.2005-1167

16. Schwer, D., and Kailasanath, K. "Effect of Inlet on Fill Region and Performance of Rotating Detonation Engines," *47th AIAA/ASME/SAE/ASEE Joint Propulsion Conference & Exhibit*. 2011, 6044.
doi:10.2514/6.2011-6044

17. Nordeen, C., Schwer, D., Schauer, F., Hoke, J., Barber, T., and Cetegen, B. "Divergence and Mixing in a Rotating Detonation Engine," *51st AIAA Aerospace Sciences Meeting including the New Horizons Forum and Aerospace Exposition*. 2013, AIAA 2013-1175.
doi:10.2514/6.2013-1175

18. Nordeen, C., Schwer, D., Schauer, F., Hoke, J., Barber, T., and Cetegen, B. "Role of Inlet Reactant Mixedness on the Thermodynamic Performance of a Rotating Detonation Engine," *Shock Waves* Vol. 26, No. 4, 2016, pp. 417-428.
doi:10.1007/s00193-015-0570-7

19. Rankin, B. A., Richardson, D. R., Caswell, A. W., Naples, A. G., Hoke, J. L., and Schauer, F. R. "Chemiluminescence Imaging of an Optically Accessible Non-Premixed Rotating Detonation Engine," *Combustion and Flame* Vol. 176, 2017, pp. 12-22.
doi:10.1016/j.combustflame.2016.09.020

20. Sun, J., Zhou, J., Liu, S., and Lin, Z. "Numerical Investigation of a Rotating Detonation Engine under Premixed/Non-Premixed Conditions," *Acta Astronautica* Vol. 152, 2018, pp. 630-638.
doi:10.1016/j.actaastro.2018.09.012

21. Prakash, S., Fiévet, R., and Raman, V. "The Effect of Fuel Stratification on the Detonation Wave Structure," *AIAA Scitech 2019 Forum*. 2019, AIAA 2019-1511.
doi:10.2514/6.2019-1511

22. Yi, T.-H., Turangan, C., Lou, J., Wolanski, P., and Kindracki, J. "A Three-Dimensional Numerical Study of Rotational Detonation in an Annular Chamber," *47th AIAA Aerospace Sciences Meeting including the New Horizons Forum and Aerospace Exposition*. 2009, AIAA 2009-634.
doi:10.2514/6.2009-634

23. Shao, Y.-T., Liu, M., and Wang, J.-P. "Numerical Investigation of Rotating Detonation Engine Propulsive Performance," *Combustion Science and Technology* Vol. 182, No. 11-12, 2010, pp. 1586-1597.
doi:10.1080/00102202.2010.497316

24. Schwer, D., and Kailasanath, K. "Numerical Investigation of Rotating Detonation Engines," *46th AIAA/ASME/SAE/ASEE Joint Propulsion Conference & Exhibit*. 2010, AIAA 2010-6880.
doi:10.2514/6.2010-6880

25. Pinaki, P., Gaurav, K., Scott. A. Drennan, and Brent, A. R. "Multidimensional Numerical Simulations of Reacting Flow in a Non-Premixed Rotating Detonation Engine," *Proceedings of ASME Turbo Expo 2019: Turbomachinery Technical Conference and Exposition*, 2019, pp. GT2019-91931.

26. Hishida, M., Fujiwara, T., and Wolanski, P. "Fundamentals of Rotating Detonations," *Shock Waves* Vol. 19, No. 1, 2009, pp. 1-10.
doi:10.1007/s00193-008-0178-2

27. Mahmoudi, Y., Karimi, N., Deiterding, R., and Emami, S. "Hydrodynamic Instabilities in Gaseous Detonations: Comparison of Euler, Navier–Stokes, and Large-Eddy Simulation," *Journal of Propulsion and Power* Vol. 30, No. 2, 2014, pp. 384-396.
doi:10.2514/1.B34986

28. Zhdan, S. A., Bykovskii, F. A., and Vedernikov, E. F. "Mathematical Modeling of a Rotating Detonation Wave in a Hydrogen-Oxygen Mixture," *Combustion, Explosion, and Shock Waves* Vol. 43, No. 4, 2007, pp. 449-459. doi:10.1007/s10573-007-0061-y

29. Davidenko, D., Gökalp, I., and Kudryavtsev, A. "Numerical Study of the Continuous Detonation Wave Rocket Engine," *15th AIAA International Space Planes and Hypersonic Systems and Technologies Conference*. 2008, AIAA 2008-2680.
doi:10.2514/6.2008-2680

30. Yi, T.-H., Lou, J., Turangan, C., Choi, J.-Y., and Wolanski, P. "Propulsive Performance of a Continuously Rotating Detonation Engine," *Journal of Propulsion and Power* Vol. 27, No. 1, 2011, pp. 171-181.
doi:10.2514/1.46686

31. Schwer, D., and Kailasanath, K. "Numerical Investigation of the Physics of Rotating-Detonation-Engines," *Proceedings of the Combustion Institute* Vol. 33, No. 2, 2011, pp. 2195-2202.
doi:10.1016/j.proci.2010.07.050

32. Rankin, B. A., Fotia, M., Paxson, D. E., Hoke, J., and Schauer, F. "Experimental and Numerical Evaluation of Pressure Gain Combustion in a Rotating Detonation Engine," *53rd AIAA Aerospace Sciences Meeting*. 2015, AIAA 2015-0877.
doi:10.2514/6.2015-0877

33. Paxson, D. E., Fotia, M., Hoke, J., and Schauer, F. "Comparison of Numerically Simulated and Experimentally Measured Performance of a Rotating Detonation Engine," *53rd AIAA Aerospace Sciences Meeting*. 2015, AIAA–2015–1101.
doi:10.2514/6.2015-1101

34. Fujii, J., Kumazawa, Y., Matsuo, A., Nakagami, S., Matsuoka, K., and Kasahara, J. "Numerical Investigation on Detonation Velocity in Rotating Detonation Engine Chamber," *Proceedings of the Combustion Institute* Vol. 36, No. 2, 2017, pp. 2665-2672.
doi:10.1016/j.proci.2016.06.155

35. Shank, J., King, P., Karnesky, J., Schauer, F., and Hoke, J. "Development and Testing of a Modular Rotating Detonation Engine," *50th AIAA Aerospace Sciences Meeting including the New Horizons Forum and Aerospace Exposition*. 2012, AIAA 2012-0120.
doi:10.2514/6.2012-120

36. D. M. G. Gregory P. Smith, M. F., Nigel W. Moriarty, Boris Eiteneer, Mikhail Goldenberg, C. Thomas Bowman, Ronald K. Hanson, Soonho Song, William C. Gardiner, Jr., Vitali V. Lissianski, and Zhiwei. "GRI-Mech 3.0. Available: http://www.me.berkeley.edu/gri_mech/."

37. Menter, F. R. "Two-Equation Eddy-Viscosity Turbulence Models for Engineering Applications," *AIAA Journal* Vol. 32, No. 8, 1994, pp. 1598-1605.
doi:10.2514/3.12149

38. Van Leer, B. "Towards the Ultimate Conservative Difference Scheme. V. A Second-Order Sequel to Godunov's Method," *Journal of Computational Physics* Vol. 32, No. 1, 1979, pp. 101-136.
doi:10.1016/0021-9991(79)90145-1

39. Stephen, R. T. "Chemical Kinetics", *An Introduction to Combustion: Concepts and Applications*. McGraw-hill, New York, 2000, pp. 111-143.

40. Goodwin, D. G., Moffat, H. K., and Speth, R. L. "Cantera: An object-oriented software toolkit for chemical kinetics, thermodynamics, and transport processes," *Caltech, Pasadena, CA*, 2009.

41. Lee, J. H. "Gas Dynamic Theory of Detonations and Deflagarations", *The Detonation Phenomenon*. Cambridge University Press, New York, 2008, pp. 26-52.

42. Coleman, T. F., and Li, Y. "On the Convergence of Interior-Reflective Newton Methods for Nonlinear Minimization Subject to Bounds," *Mathematical Programming* Vol. 67, No. 1-3, 1994, pp. 189-224.
doi:10.1007/BF01582221

43. Coleman, T. F., and Li, Y. "An Interior Trust Region Approach for Nonlinear Minimization Subject to Bounds," *SIAM Journal on Optimization* Vol. 6, No. 2, 1996, pp. 418-445.
doi:10.1137/0806023

44. Pudsey, A. S., and Boyce, R. R. "Numerical Investigation of Transverse Jets through Multiport Injector Arrays in a Supersonic Crossflow," *Journal of Propulsion and Power* Vol. 26, No. 6, 2010, pp. 1225-1236.
doi:10.2514/1.39603

45. Driscoll, R., George, A. S., and Gutmark, E. J. "Numerical Investigation of Injection within an Axisymmetric Rotating Detonation Engine," *International Journal of Hydrogen Energy* Vol. 41, No. 3, 2016, pp. 2052-2063.
doi:10.1016/j.ijhydene.2015.10.055

46. Celik, I. B., Ghia, U., and Roache, P. J. "Procedure for Estimation and Reporting of Uncertainty due to Discretization in CFD applications," *Journal of Fluids Engineering* Vol. 130, No. 7, 2008, pp. 078001–078004.

47. Andrus, I. Q. "A Premixed Rotating Detonation Engine: Design and Experimentation," *Dissertation*. Air Force Institute of Technology, 2016.

48. Zhdan, S., and Syryamin, A. "Numerical Modeling of Continuous Detonation in Non-Stoichiometric Hydrogen-Oxygen Mixtures," *Combustion, Explosion, and Shock Waves* Vol. 49, No. 1, 2013, pp. 69-78.
doi:10.1134/S0010508213010085

49. Shepherd, J. "Detonation in Gases," *Proceedings of the Combustion Institute* Vol. 32, No. 1, 2009, pp. 83-98.
doi:10.1016/j.proci.2008.08.006

50. Powers, J. M. "Review of Multiscale Modeling of Detonation," *Journal of Propulsion and Power* Vol. 22, No. 6, 2006, pp. 1217-1229.
doi:10.2514/1.17897

51. Powers, J. M., and Paolucci, S. "Accurate Spatial Resolution Estimates for Reactive Supersonic Flow with Detailed Chemistry," *AIAA Journal* Vol. 43, No. 5, 2005, pp. 1088-1099.
doi:10.2514/1.11641

52. Prakash, S., Fiévet, R., Raman, V., Burr, J. R., and Yu, K. H. "Numerical Study of the Detonation Wave Structure in a Linear Model Detonation Engine," *2018 Joint Propulsion Conference*. 2018, AIAA 2018-4966.
doi:10.2514/6.2018-4966

53. Wu, M., and Martin, M. P. "Direct Numerical Simulation of Supersonic Turbulent Boundary Layer over a Compression Ramp," *AIAA Journal* Vol. 45, No. 4, 2007, pp. 879-889.
doi:10.2514/1.27021

54. Nordeen, C. A., Schwer, D., Schauer, F., Hoke, J., Barber, T., and Cetegen, B. "Thermodynamic model of a rotating detonation engine," *Combustion, Explosion, and Shock Waves* Vol. 50, No. 5, 2014, pp. 568-577.

55. Schwer, D., and Kailasanath, K. "Numerical Study of the Effects of Engine Size on Rotating Detonation Engines," *49th AIAA Aerospace Sciences Meeting Including the New Horizons Forum and Aerospace Exposition*. 2011, AIAA 2011-581.
doi:10.2514/6.2011-581

56. Austin, J., and Shepherd, J. "Detonations in Hydrocarbon Fuel Blends," *Combustion and Flame* Vol. 132, No. 1-2, 2003, pp. 73-90.
doi:10.1016/S0010-2180(02)00422-4

57. Vasil'Ev, A., Mitrofanov, V., and Topchiyan, M. "Detonation Waves in Gases," *Combustion, Explosion and Shock Waves* Vol. 23, No. 5, 1987, pp. 605-623.
doi:10.1007/BF00756541

58. Hebral, J.-P., and Shepherd, J. "User Guide for Detonation Cell Size Measurement using Photoshop and Matlab," *Explosion Dynamics Laboratory Report FM00-6*. California Institute of Technology, Pasadena, CA, 2000, (http://shepherd.caltech.edu/EDL/PublicResources/CellImageProcessing/cellsize/Userguide.pdf).

59. Ciccarelli, G., Ginsberg, T., Boccio, J., Economos, C., Sato, K., and Kinoshita, M. "Detonation Cell Size Measurements and Predictions in Hydrogen-Air-Steam Mixtures at Elevated Temperatures," *Combustion and Flame* Vol. 99, No. 2, 1994, pp. 212-220.
doi:10.1016/0010-2180(94)90124-4

Appendices

Appendix A – Code for the weighted random number generator

The following section is the Java code (macro) used to generate weighted random numbers and append it as a boundary condition to the 2-D simulation in Star-CCM+.

Note:

1. In line 80 of the code, the variable '*no_of_cells*' is to be changed according to the number of cells in the first row of the 2-D domain.
    - Example: For a cell size of 0.1 mm, the value of '*no_of_cells*' would be 4596. This is because the length of the domain is 0.4596 m.

2. The code requires three csv files:
    - *items.csv* - Has the fuel mass fractions extracted from the 3-D simulation
    - *weight.csv* - Has the weight of the numbers in the above csv
    - *x_coord.csv* – Has the x-coordinates of the cells centers (from Star-CCM+)

Code:

```
// CHANGE THE VALUE OF 'no_of_cells' IN LINE 80 BASED ON MESH SIZE (no_of_cells = 0.4596 / del_x_required)

package macro;

import java.util.*;
import star.common.*;
import star.base.neo.*;
import star.flow.*;
import star.coupledflow.*;
import star.species.*;
import star.energy.*;
import star.vis.*;
import java.io.*;
import java.util.*;
import org.openide.util.Exceptions;
import java.io.File;
import java.io.IOException;
import java.io.FileNotFoundException;
import java.io.FileWriter;
import java.io.FileReader;
import java.io.BufferedWriter;
import java.io.BufferedReader;
import java.util.ArrayList;
import java.util.Arrays;
import java.util.Collections;
import java.util.Random;
import java.util.Scanner;
import java.lang.StringBuilder;
```

```
public class SMA_2D_RNG_finer extends StarMacro {

  public void execute() {
    execute0();
  }

  private void execute0() {

    Simulation simulation_0 =
      getActiveSimulation();

FileTable fileTable_2 =
        (FileTable) simulation_0.getTableManager().createFromFile(resolvePath("Inlet_BC_mfs.csv"));

Region region_0 =
         simulation_0.getRegionManager().getRegion("Region");

Boundary boundary_0 =
        region_0.getBoundaryManager().getBoundary("2D_RDE.Inlet");

MassFractionProfile massFractionProfile_0 =
        boundary_0.getValues().get(MassFractionProfile.class);

ScalarProfile scalarProfile_0 =
        massFractionProfile_0.getMethod(CompositeArrayProfileMethod.class).getProfile(1);

scalarProfile_0.getMethod(XyzTabularScalarProfileMethod.class).setTable(fileTable_2);

scalarProfile_0.getMethod(XyzTabularScalarProfileMethod.class).setData("Mass Fraction of H2");

ScalarProfile scalarProfile_2 =
          massFractionProfile_0.getMethod(CompositeArrayProfileMethod.class).getProfile(7);
```

```
scalarProfile_2.getMethod(XyzTabularScalarProfileMethod.class).setTable(fileTable_2);

scalarProfile_2.getMethod(XyzTabularScalarProfileMethod.class).setData("Mass Fraction of O2");

ScalarProfile scalarProfile_1 =
          massFractionProfile_0.getMethod(CompositeArrayProfileMethod.class).getProfile(5);

scalarProfile_1.getMethod(XyzTabularScalarProfileMethod.class).setTable(fileTable_2);

scalarProfile_1.getMethod(XyzTabularScalarProfileMethod.class).setData("Mass Fraction of N2");


/*----RNG initial step------*/

Random r = new Random();
int no_of_cells = 4596;    //----- No of cells in the first row of the 2-D geometry --------------------

//------------ Declare output variables ----------------------------------------------------------------

        double[] H2_BC = new double[no_of_cells];
        double[] N2_BC = new double[no_of_cells];
        double[] O2_BC = new double[no_of_cells];

//------------ Declaration -----------------------------------------------------------------------------

        File items, weights, xc_file;
        Scanner s, s1, xc;
        ArrayList<Double> weightList, itemList, h2mf, xcoord;
        Double nextElement, High, weight, item, Low, randomValue, x_c;

        String items_file = simulation_0.getSessionDir() + File.separator + "items.csv";
        String weights_file = simulation_0.getSessionDir() + File.separator + "weight.csv";
        String xcs_file = simulation_0.getSessionDir() + File.separator + "x_coord.csv";
```

```
        String bc_file = simulation_0.getSessionDir() + File.separator + "Inlet_BC_mfs.csv";

//----------- Get the Items and weight list ----------------------------------------------------------------

                items = new File(items_file);
                weights = new File(weights_file);
                xc_file = new File(xcs_file);

                weightList = new ArrayList<>();
                itemList = new ArrayList<>();
                h2mf = new ArrayList<>();

                try{

                s = new Scanner(weights);
                s1 = new Scanner(items);

            while(s.hasNext()){
                weight = s.nextDouble();         //Sum of all weights is 1
                weight = weight*no_of_cells;
                weightList.add(weight);
            }

            while(s1.hasNext()){
                item = s1.nextDouble();
                itemList.add(item);
            }

                        nextElement = itemList.get(0);
                        High = itemList.get(1);

                        xc = new Scanner(xc_file);
                        xcoord = new ArrayList<>();
```

```
                        while(xc.hasNext()){
                                x_c = xc.nextDouble();
                                xcoord.add(x_c);
                        }

                int count = 1;
                                        for(int i = 0;i<weightList.size();i++){
                                                for(int j=0;j<(Math.round(weightList.get(i)));j++){
                                                        Low = nextElement;
                                                        randomValue = Low + ((High - Low) * r.nextDouble());
                                                        h2mf.add(randomValue);
                                                }
                                                nextElement = High;
                                                count++;
                                                        if(count<itemList.size()){
                                                        High = itemList.get(count);
                                                }
                                        }

                                        h2mf.add(High);

//------------ Shuffle the random numbers among different cells ------------------------------------------

                                        for(int k=1; k<100000000; k++){
                                        simulation_0.getSimulationIterator().run(3);
                                        Integer[] index = new Integer[no_of_cells];
                                                for (int i =0;i<no_of_cells;i++){
                                                        index[i] = i;
                                                }
                                                Collections.shuffle(Arrays.asList(index));

                                        for (int i=0;i<no_of_cells;i++){
```

```
                                                            H2_BC[i] = h2mf.get(index[i]);
                                                            N2_BC[i] = 0.77*(1-H2_BC[i]);
                                                            O2_BC[i] = 0.23*(1-H2_BC[i]);
                                                    }

FileWriter fw = new FileWriter(bc_file);
BufferedWriter br = new BufferedWriter(fw);

StringBuilder sb = new StringBuilder();
sb.append("\"Mass Fraction of H2\"").append(",").append("\"Mass Fraction of O2\"").append(",").append("\"Mass
Fraction of N2\"").append(",").append("\"X (m)\"").append(",").append("\"Y (m)\"").append(",").append("\"Z
(m)\"").append("\n");

for (int i=1;i<=no_of_cells;i++){
sb.append(H2_BC[i-1]).append(",").append(O2_BC[i-1]).append(",").append(N2_BC[i-
1]).append(",").append(xcoord.get(i-1)).append(",").append(0).append(",").append(0);
sb.append("\n");
}
                        br.write(sb.toString());
                        br.close();

                fileTable_2.extract();

                }
                }

                catch (IOException e) {
                        simulation_0.println("Error in Secion");
                        e.printStackTrace();
                        }

  }
}
```

Appendix B – Code to calculate theoretical CJ velocity

Note:

- Include the mechanism file to be used. In this case it is the GRI mechanism. It should be in .ci format

Code:

```
%State 1
T1 = 298; %K
P1 = 101325; %Pa
X = [0,0.5,0.5*3.76];

T2_guess = 3000;
P2_guess = 2.0e6;
Vd_guess = 1900;

y_guess = [T2_guess,P2_guess,Vd_guess];

q = 0;
F = @(y)CJ_calc(y,P1,T1,X,q);
out = fsolve(F,y_guess)

T2 = out(1);
P2 = out(2);
Vd = out(3);
```

```
function [F] = CJ_calc(Y,P1,T1,X,q)
    T2 =Y(1);
    P2 = Y(2);
    Vd = Y(3);

    gas1 = IdealGasMix('GRI.cti');
    nsp = nSpecies(gas1);
    ih2 = speciesIndex(gas1,'H2');
    io2 = speciesIndex(gas1,'O2');
    ich4 = speciesIndex(gas1,'CH4');
    in2 = speciesIndex(gas1,'N2');

    x = zeros(nsp,1);
    x(ich4,1)  = X(1);
    x(ih2,1) = 1-X(1);
    x(io2,1) = X(2);
    x(in2,1) = X(3);

    set(gas1,'Temperature',T1,'Pressure',P1,'MoleFractions', x);
    gas2 = IdealGasMix('GRI.cti');
    set(gas2,'Temperature',T2,'Pressure',P2,'MoleFractions',x);
    equilibrate(gas2,'TP');

    R2 = 8314/meanMolecularWeight(gas2);
    gamma2 = cp_mass(gas2)/cv_mass(gas2);
    density2 = density(gas2);
    u2 = intEnergy_mass(gas2);
    R1 = 8314/meanMolecularWeight(gas1);
```

```
    u1 = intEnergy_mass(gas1);

    F(1) = u2-u1+q-0.5*(P2.^2-P1.^2)*(1/(gamma2*P2*density2));
    F(2) = (P1+P2)*(R1*T1/P1-R2*T2/P2)-(P2^2-P1^2)*(R2*T2/(gamma2*P2^2));
    F(3) = Vd-(P2*R1*T1)/(P1*R2*T2)*sqrt(gamma2*R2*T2);
end
```